



HAL
open science

Gas concentration and flow rate measurements as part of methane baseline assessment: Case of the Fontaine Ardente gas seep, Isère, France

Frédéric Gal, Wolfram Kloppmann, Eric Proust, Pauline Humez

► To cite this version:

Frédéric Gal, Wolfram Kloppmann, Eric Proust, Pauline Humez. Gas concentration and flow rate measurements as part of methane baseline assessment: Case of the Fontaine Ardente gas seep, Isère, France. *Applied Geochemistry*, 2018, 95, pp.158-171. 10.1016/j.apgeochem.2018.05.019 . hal-02860753

HAL Id: hal-02860753

<https://brgm.hal.science/hal-02860753>

Submitted on 21 Nov 2023

HAL is a multi-disciplinary open access archive for the deposit and dissemination of scientific research documents, whether they are published or not. The documents may come from teaching and research institutions in France or abroad, or from public or private research centers.

L'archive ouverte pluridisciplinaire **HAL**, est destinée au dépôt et à la diffusion de documents scientifiques de niveau recherche, publiés ou non, émanant des établissements d'enseignement et de recherche français ou étrangers, des laboratoires publics ou privés.

1 Gas concentration and flow rate measurements as part of methane baseline assessment:
2 Case of the Fontaine Ardente gas seep, Isère, France.

3

4 Authors:

5 Gal F.^{1*}, Kloppmann W.¹, Proust E.¹, Humez P.²

6

7 1: BRGM, 3 Avenue Claude Guillemin, 45060 Orléans, France

8 2: University of Calgary, Department of Geoscience, Calgary, Alberta, Canada

9 *: corresponding author: f.gal@brgm.fr

10 **Abstract**

11 Methane and CO₂ gas emissions from a gas seep located in the French Alps, documented
12 over two millenaries, have been quantified along with gas emissions from the miniseepage
13 area contouring the main vent. Several tons per year of both gas phases are released in the
14 atmosphere from the main seep (18 tons of CH₄ and 5.5 tons of CO₂) which has been
15 modified by an old borehole. Diffuse seepage brings additional CH₄ (1 ton per year) and CO₂
16 (2.3 tons per year) which are emitted from a small area of 240 m². Secondary CH₄ oxidation
17 processes are likely to occur near the surface. Biologically produced CO₂ is also found in the
18 soil in the seepage area and the biological component becomes predominant as CO₂
19 concentrations drop lower than 2% vol. Soil gas CH₄+CO₂ enrichments are oriented along
20 N45 and N170 pathways that represent the main structural directions of the area. Soil flux
21 anomalies are more scattered because surface clay formations have been strongly reworked
22 at surface. Variety of methods (IRGA, micro-GC, accumulation chamber flux measurements,
23 IR-camera) were tested and are discussed in connection with environmental impact
24 monitoring and the role of sampling conditions, with emphasis on shale gas and carbon
25 storage baseline assessments The role of potential leakage pathways represented by the old
26 borehole structure is also discussed as an analogue with leaky shale gas wells.

27 **Highlights**

- 28 - Definition of the degassing pattern of a major CH₄+CO₂ gas seep in the French Alps.
- 29 - Quantification of greenhouse gas emissions to the atmosphere from this gas seep.
- 30 - Implications for containment and environmental baseline assessment related to
- 31 shale gas environmental impact.

32

33 **Keywords**

34 Methane – gas seep – natural degassing – environmental baseline assessment – shale gas

35 **1. Introduction**

36 Natural Earth degassing is a matter of concern and investigation since many years in various
37 fields such as volcanology or geothermics. Often relying on the characterization of the gas
38 species percolating from depth to shallow horizons and subsequently to the atmosphere,
39 these studies have provided better constraints on the sources and amounts of gases
40 released to the atmosphere and on potential migration pathways. Numerous studies have
41 dealt with the evaluation of the amounts of CO₂ and other gases naturally released by
42 volcanic structures (e.g. Greenland *et al.*, 1985; Hobbs *et al.*, 1991; Brantley and Koepenick,
43 1995; Halmer *et al.*, 2002) and the consequences such releases may have on human health
44 (e.g. Sigurdsson *et al.*, 1987; Baxter *et al.*, 1999). Gas emissions from geothermal areas and
45 from geothermal exploitation have also received growing interest as contribution to
46 greenhouse gases (GHG) in the atmosphere (e.g. Capaccioni *et al.*, 1993; Cardenelli *et al.*,
47 2003a; Armannsson *et al.*, 2005). Furthermore, they induce direct risks for human dwellings
48 (e.g. Durand and Scott, 2005). Gas releases may also be associated with emissions from
49 hydrothermal resources (e.g. Battani *et al.*, 2010), from non-volcanic areas (e.g. Rogie *et al.*,
50 2000) or from other subsoil reservoirs (e.g. Etiope and Martinelli, 2002; Voltattorni and
51 Lombardi, 2010): they are associated with mud volcanoes (e.g. Jud, 2005; Etiope *et al.*,
52 2011a) and with hydrocarbon plays (e.g. Etiope, 2015). The budgets of carbon emissions to
53 the atmosphere have been assessed in the 2000's (e.g. Mörner and Etiope, 2002) and are
54 regularly refined for CO₂ (e.g. Holloway *et al.*, 2007) or CH₄ (e.g. Etiope, 2015). Recently,
55 methane emissions from igneous rocks (abiotic gas) have also been recognized as more
56 widespread and more important than previously thought (e.g. Etiope, 2017).

57 Consequently, there is still need to better constrain methane emissions to the atmosphere
58 given its elevated greenhouse power. As pointed out by Etiope (2015) in his landmark
59 monograph, the importance of hydrocarbon seepage from onshore locations is far from
60 negligible. The refinement of natural gas seepage contributions to the atmospheric methane
61 budget thus contributes to better understanding the impacts on climatic forcing.
62 Hydrocarbons released by gas seeps, miniseepages, microseepages and emissions from mud
63 volcanoes are phenomena occurring worldwide, in Europe (Germany, Greece, Italy,
64 Romania, Switzerland), Azerbaijan, Turkey, Asia (China, Japan, Taiwan), Australia and USA.
65 Emissions from ophiolites or igneous intrusions (Etiope, 2015) are even more widespread.
66 Methane seeps are also an important part of the geochemical baseline that needs to be
67 defined when assessing the environmental impact of conventional and unconventional
68 hydrocarbon exploration and exploitation (Humez *et al.*, 2016; Mayer *et al.*, 2015; Mayer *et*
69 *al.*, 2016).

70 Emissions of alkanes in the alpine foreland are reported in Switzerland (Giswil, Northern
71 Alps; Etiope *et al.*, 2010) taking the form of both diffuse degassing area and gas vents with
72 large amounts of thermogenic gas released each year (more than 16 tons per year from 2
73 main seeps and diffuse degassing). Gas seeps in France are largely under-investigated
74 (Etiope, 2009). Only one site is mentioned in the MAGA database
75 (http://www.magadb.net/global_map/) even though methane point emissions do not seem
76 to be an uncommon phenomenon in the French Subalpine Chains (Figure 1), apparently
77 systematically related to outcropping or underlying Lower Jurassic argillaceous sediments.

78 We report investigations at the most prominent French alpine gas seep, known for at least
79 two millenaries, the Fontaine Ardente du Gua site, south of Grenoble (hereafter referred to

80 as Fontaine Ardente). First measurements, in June 2015, aimed to define the shape of the
81 gas emissions at surface and preliminary results can be found in Kloppmann *et al.* (2016) and
82 in Gal *et al.* (2017a). Here we present more detailed investigations based on soil gas
83 measurements and on soil gas flux measurements performed in October 2016, allowing a
84 first quantitative assessment of CH₄ and CO₂ fluxes to the atmosphere.

85 Figure 1

86

87 **2. Geological and historical settings**

88 The Fontaine Ardente gas seep is situated 20 km South-West from Grenoble city (Isère
89 department, France), at the foothill of the Urgonian limestone cliffs of the Vercors Massif
90 (Figure 1**Error! Reference source not found.**). The gas emanates from Callovian claystones
91 and argillaceous limestones (black shales) in a small thalweg in the main bed of the Vernant
92 creek. Gas escapes are thought to be linked with faults but the geometry of these faults
93 remains unclear and so does the origin of the gas phase. There has been a debate between a
94 deep origin, linked to the existence of a deep fault reaching Triassic formations, and a near
95 surface origin, linked to a minor fault only affecting shales (Mercier and Seguin, 1939), the
96 region being rich in organic-rich sediments (coal seams of La Mûre or the Motte d'Aveillans
97 coalfield; Berthier *et al.*, 1991).

98 The Fontaine Ardente seep is known from ancient times (as early as 426 AD) as “burning
99 water” because the seep was initially observed in the stream bed of the Vernant creek
100 (Figure 1). Following the rush in hydrocarbons exploitation in the US (especially in
101 Pennsylvania) and Canada in the XIXth century, pro-parte based on the discovery of natural

102 gas associated with hydrocarbons, attempts to exploit the Fontaine Ardente gas have been
103 made around 1880 (Piret, 1881). It was believed that there must be a considerable gas
104 reservoir together with perennial gas production to allow leakage of methane at ground
105 surface for such a long time – a volume of $1.73 \times 10^3 \text{ m}^3$ (3.1 tons at boiling point) of CH_4 per
106 day was evaluated in the late XIXth century.

107 The composition of the gas phase was analyzed for the first time at the end of the XIXth
108 century: 98.81% (vol.) of CH_4 , 0.58% of CO_2 , 0.48% of N_2 , 0.10% of O_2 and 0.03% of loss or
109 bias during analysis (Piret, 1881). It was reevaluated in 1960, leading to the sole detection of
110 CH_4 and CO_2 at 91.16% and 8.84% respectively (cited in AHPG, 2012). Traces of O_2 and N_2
111 previously described were attributed to atmospheric contamination during sampling.

112 In view of the exploitation of the gas phase, the primitive site was profoundly modified in
113 the goal of focusing the patchy gas emissions into a unique emitting point (Piret, 1881).
114 Infrastructure was built to deviate stream water and to allow the construction of a
115 gasometer to collect gas without interaction with surface waters. From this gasometer the
116 gas was piped uphill for further use to the plateau surrounding the thalweg where the
117 fountain is located. The exploitation quickly ceased as the gas production could not be
118 enhanced and floods repeatedly destroyed the surface infrastructure. The investigations
119 related to these works concluded that the rock formations near the surface were altered
120 down to a depth of 18 to 20 m below ground surface by the long-term percolation of the
121 gas. Due to flooding in 1956, the site was covered by detrital sediments, the gas emission
122 pathways have changed and the gas flux to the surface decreased.

123 In order to enhance and better constrain gas emissions, further works were undertaken in
124 the 90's (Berthier *et al.*, 1991). After surveying soil gas (CO_2 soil gas concentration

125 prospecting at 0.5 m depth), 2 boreholes (FA1 and FA2) were drilled down to 35 m below
126 ground level. Only one (FA2; Figure 1) was methane rich, main gas inflow occurring at about
127 10 m depth. Gas flowrate was measured at 130 l/min at 0.1 bars during 3 hours (borehole
128 opened). Once closed, borehole pressure increased up to 0.6 bars. Exploitation of the gas
129 had been expected to be possible at above 90 l/min but no exploitation was tried. Nowadays
130 the FA2 borehole represents the main seep knowing that the wellhead has been destroyed
131 and that additional reworking led to the building of a concrete platform around the former
132 wellhead and to the flattening of the area close to FA2 borehole as shown by Figure 1 **Error!**
133 **Reference source not found..**

134

135 **3. Methods**

136 Site investigations at Fontaine Ardente used two approaches: soil gas concentrations
137 measurements at 1 m depth and soil gas flux quantification at the soil/atmosphere interface.

138 **3.1. Soil gas measurements**

139 Soil gas concentrations were measured according to a well-established methodology used
140 *e.g.* for monitoring for Carbon Capture and Storage (CCS) sites (Gal *et al.*, 2014). A 1 m
141 square mesh grid was used in 2015 (Figure 1). In 2016, the mesh grid varied from 1 x 1 m to
142 1 x 2 m. Some measurements were performed outside of this grid and outside of the
143 Vernant river bed. These points serve as reference points for the evaluation of background
144 characteristics of soil gas. Small holes (1 cm in diameter) were drilled down to 1 m depth.
145 Such a small mesh size for systematic sampling is rarely used in similar studies (*e.g.*
146 Bloomberg *et al.*, 2012) and is a direct consequence of the small size of the area to monitor.

147 Using a small mesh is also a way to lower the uncertainty in soil gas flux quantifications that
148 may be related to the use of relatively small flux chambers (Parkin and Venterea, 2010).
149 Owing to the presence of a concrete platform and surrounding rockwall (gabion wall), the
150 area cannot be monitored totally.

151 For soil gas investigations, a sampling tube was inserted into the hole of 1 cm in diameter
152 and an Infra-Red Gas Analyzer (IRGA, LFG20 by ADC Gas Analysis Ltd., UK) was plugged,
153 pumping at low flow rate ($200 \text{ ml}\cdot\text{min}^{-1}$) and reaching steady state conditions within tens of
154 seconds. No concentration changes on very short time scale (minutes) were observed. The
155 IRGA allowed a direct estimate of CH_4 , CO_2 and O_2 gas concentrations in soils. Analytical
156 precision for CO_2 and CH_4 was $\pm 0.5\%$ of the reading for low concentration range (0.01–10%
157 vol.), $\pm 3\%$ of the reading for higher concentrations (10 to 50% vol.) and up to $\pm 5\%$ of the
158 reading for the CO_2 sensor and $\pm 16\%$ for the CH_4 sensor for concentrations greater than 50%
159 (a procedure is described in supplementary information to correct the bias for CH_4
160 concentrations). The precision for oxygen was $\pm 0.4\%$ full scale reading (0–25% vol.).

161 Complementary characterization of the gas phase was performed in 2015 using gas micro-
162 chromatography (Agilent 3000) in order to increase the accuracy of CH_4 determinations (IR
163 sensors exhibit non-linear absorption at high gas concentrations). Samples were stored in
164 Tedlar[®] bags during site monitoring and analyzed by the end of the day. A quantitative
165 assessment of the gas phase composition was then possible for permanent gases (CO_2 , O_2 ,
166 N_2 , Ar), alkanes (CH_4 , C_2H_6 , C_3H_8) and ^4He . Detection limits are 10 ppm for permanent gases,
167 2 ppm for alkanes and 50 ppm for helium. Precision of the measurement is better than 2% at
168 full scale.

169

170 **3.2. Soil flux measurements**

171 Soil gas flux measurements were performed in 2016 on the 1 x 1 to 1 x 2 m mesh grid. At
172 some locations, flux monitoring was not technically feasible as the ground was too pebbly, in
173 the bed of the Vernant creek or strongly modified by the concrete platform and the rockwall
174 (Figure 1). The accumulation chamber technique, with external recirculation, was used. Such
175 closed chamber measurements are widely used for CO₂ flux quantifications (*e.g.* Chiodini *et*
176 *al.*, 1998; Fridriksson *et al.*, 2006) and are also applied to CH₄ flux measurements (*e.g.* Etiope
177 *et al.*, 2013a; Gal *et al.*, 2014). Reliable and representative estimates of the soil gas flux can
178 be obtained as this technique does not rely on corrections depending on soil characteristics
179 (Chiodini *et al.*, 1998, and references therein). The flux chamber system is a customized
180 version of the soil gas flux system of Echo Instruments (Slovenia). The aluminum chamber
181 has a semi-spherical geometry with a basal area of 0.0289 m² and a volume of 0.0018 m³
182 (soft ground) to 0.0023 m³ (hard ground). There is no anchor installation prior to
183 measurement as the sharp-edged base of the chamber is shaped to be easily inserted in the
184 ground. A fan with tunable speed ensures the required mixing of the headspace gas (Parkin
185 and Venterea, 2010). Pressure, temperature and relative humidity inside the chamber, as
186 well as pumping rate, are continuously monitored thus giving estimates on the possible
187 influence of external parameters on the measurements. The following gas species are
188 monitored: CO₂ and CH₄ by Non-Dispersive Infra-Red (NDIR) detectors (0 to 5000 ppmv ± 2%
189 and 0 to 10000 ppmv ± 5% respectively), O₂ and H₂S by electrochemical cells (0 to 25% vol. ±
190 2% of the reading and 0 to 10000 ppmv ± 5% of the reading respectively). The
191 measurements are performed directly on the soil surface without removal of the first
192 centimeters of the soil as it was sometimes reported (Fridriksson *et al.*, 2006). Around two
193 thirds of the fluxes were measured on bare soil or gravel soil, the rest on vegetated soil

194 (grass). This allowed quantification of the gas emissions to the atmosphere under
195 undisturbed conditions (soil removal may artificially enhance gas emissions if performed
196 shortly before measurement).

197 The flux measurement was based on the rate of CH₄ and CO₂ increases (positive fluxes), and
198 possible opposite O₂ decrease (“negative” fluxes), in the chamber. Usually positive values
199 indicate fluxes directed from the soil to the atmosphere and negative values indicate flow
200 from the atmosphere into the soil (*e.g.* D'Alessandro *et al.*, 2018). Details on the procedure
201 used to calculate flux is given as supplementary information.

202

203 **4. Results and discussion**

204 **4.1. Meteorological conditions**

205 The influence of meteorological conditions is a widely reported phenomenon (*e.g.* Toutain
206 and Baubron, 1999). The two campaigns were performed under contrasted climatic
207 conditions.

208 In June 2015, high rainfall amounts were recorded prior to the field acquisitions (40 mm on
209 June 13 and 14). Such amounts can lower the soil gas concentrations in the upper part of the
210 soil (0 to 40 cm depth) – and so the gas flux at the soil/atmosphere interface – as the result
211 of a barrier effect that reduces gas emissions to the surface when water is percolating
212 downwards and/or dissolving part of the soil CO₂ (Hinkle, 1994). At the opposite, increases
213 of the concentrations by a “piston” accumulation effect can be observed deeper in the soil
214 (Bouma and Bryla, 2000). Rainfall has less influence on CH₄ as it is less soluble in water than
215 CO₂ (Weiss, 1974; Wiesenburg and Guinasso, 1979). Gas emission can also be affected by

216 pressure variations with possible anti-correlation of gas with air pressure (Toutain and
217 Baubron, 1999) even if this relation has not been observed in all cases (*e.g.* Gal *et al.*, 2014).

218 The situation was opposite in October 2016. Only 4 mm of rainfall occurred during the two
219 days preceding the measurements and August and September 2016 were drought months
220 (only 37.8 + 37.1 mm precipitated compared to 67.2 + 105.7 mm on thirty-year average;
221 <http://www.meteofrance.com/climat/france/grenoble/38384001/relevés>). Influence of
222 rainfalls on gas emissions may be of secondary importance in 2016 as water uptake by
223 vegetation and/or evaporation after rainfalls may preclude water to percolate deep in the
224 soil. This period of drought also allowed enlarging the monitoring area by performing some
225 data acquisitions directly in the river bed of the Vernant creek (Figure 1).

226

227 **4.2. Statistical parameters**

228 Main statistical characteristics of soil gas concentrations measured in the field by gas
229 chromatography in 2015 and IRGA in 2016 are reported in Figure 2. The 2016 IRGA data
230 were completed by some gas chromatography measurements (N_2 , 4He and C_2H_6) in order to
231 cross-check high CH_4 concentrations measured by IRGA. The gas phases monitored in 2015
232 (Gal *et al.*, 2017a) and the gas phases monitored in 2016 are in good agreement:

- 233 - Soil gas concentrations cover a wide range of variation typically linked to the
234 existence of a gas vent. Concentrations of the predominant gas in the main vent
235 (CH_4) ranged from zero up to 90% vol.

- 236 - CO₂ exists across all the monitoring area with maximum values around 11% for the
237 main vent and background values in the surrounding forest soils around 0.2% (Figure
238 1).
- 239 - Trace gases are detected less frequently. C₂H₆ and ⁴He appeared to be detectable in
240 half of the samples in 2015 and their concentrations reached respectively 590 and
241 250 ppm. In a few samples, having a composition similar to that of the main seep
242 (FA2 in Figure 1), very low amounts of C₃H₈ were measured close to the instrumental
243 detection limit (2 to 3 ppm in the present case). Interestingly, H₂S has not been
244 detected in 2015 but has been monitored at high concentrations in 2016 in four
245 samples (up to 2.2% vol. in two samples; around 200 ppm in two other samples;
246 below detection limit – 50 ppm – in the two last samples).
- 247 - Oxygen and N₂ concentrations varied from atmospheric concentrations down to near
248 zero values for O₂ and residual content for N₂. The gas emitted at the main seep is
249 composed by 89% CH₄, 9 to 9.5% CO₂, 1% residual N₂ and traces of Ar (less than
250 0.07%), ⁴He (0.018%) and C₂H₆ (0.0002%). H₂S measured in 2016 accounts for
251 additional 2% vol. These values well match with the corrected IRGA measurements
252 (respectively 92-93% CH₄, 9-9.2% CO₂ and 0% O₂). By comparison, a smaller gas seep
253 reported locally (Meylan-Rochasson gas seep; Gal *et al.*, 2017a) is richer in CH₄
254 (94.5%), in C₂H₆ (1.9%) and C₃H₈ (0.3%), and has lower N₂ residual amount (0.35%),
255 lower ⁴He (0.007%) and CO₂ contents (0.39%).

256 Main statistical characteristics of soil gas fluxes measured in 2016 are reported in Figure 2.
257 Oxygen decrease over the duration of flux measurements (not reported in Figure 2) were
258 measured on 9 points (of 69) and ranged between -3.5 and -20 g/m²/h. Both CO₂ and CH₄

259 fluxes reached values close to 16 to 17 g/m²/h at maximum. A CO₂ flux was always possible
260 to monitor whereas CH₄ fluxes were measurable only on the four-fifths of the data.

261 Figure 2

262

263 **4.3. Data analysis**

264 All the gas concentrations measured in the soil are linearly correlated for all measured
265 parameters (Gal *et al.*, 2017a):

- 266 - Strong positive correlations were found between CH₄ and ⁴He in 2015 (Pearson's
267 coefficient of correlation of 0.970), CH₄ and C₂H₆ (0.981) and ⁴He and C₂H₆ (0.945);
- 268 - Weaker albeit statistically significant correlations were found between in 2015
269 between N₂ and O₂ (0.756), CO₂ and C₂H₆ (0.591), CO₂ and ⁴He (0.587) and in 2015
270 and 2016 between CO₂ and CH₄ (0.738);
- 271 - Reversely, strong anti-correlations were found in 2015 between N₂ and CH₄ (-0.989),
272 N₂ and C₂H₆ (-0.988) and N₂ and ⁴He (-0.960);
- 273 - Last, reverse correlations were also found in 2015 between O₂ and ⁴He (-0.794), O₂
274 and C₂H₆ (-0.755), N₂ and CO₂ (-0.610) and in 2015 and 2016 between O₂ and CO₂ (-
275 0.910) and O₂ and CH₄ (-0.810),
- 276 - Additional quantification of CO₂ and CH₄ fluxes allowed to add the following
277 tendencies: strong correlation between CO₂ and CH₄ fluxes (0.918) but neither
278 relation of CH₄ flux with CH₄ concentrations in soil gas (0.115) nor of CO₂ flux with
279 CO₂ concentrations (0.014) when considering the whole dataset.

280 Among the dataset, about two thirds of the data clearly showed the influence of the gas
281 seep (high CH₄, presence of ⁴He, C₂H₆ and CO₂).

282

283 **4.3.1. CO₂-O₂ relationship**

284 One of the most frequently studied relationships in soil gas studies is CO₂ vs. O₂ (*e.g.*
285 Romanak *et al.*, 2012; Figure 3). Three main mechanisms result in linear correlations of both
286 gases. By order of increasingly negative slopes of O₂ vs. CO₂ lines (Figure 3A), these are i)
287 dilution, occurring when a deep CO₂ endmember dilutes the O₂+N₂ pool in near surface
288 environments (slope of -0.2); ii) replacement, due to aerobic respiration in soil that
289 consumes 1 mole of O₂ to produce 1 mole of CO₂ (slope of -1) ; iii) CH₄ oxidation in near
290 surface environments where 2 moles of O₂ are needed to produce one mole of CO₂+H₂O
291 (slope of -2). The linear regression line calculated using the 2015 and the 2016
292 measurements has a slope (-2.07) very close to this CH₄ oxidation line albeit data scattering
293 is not negligible for CO₂ concentrations exceeding 3 to 4% vol. This suggests that CH₄
294 oxidation plays an important role in the appearance of CO₂ in the soil gas even if, in 2016,
295 concentrations up to 4 to 5% of CO₂ (in the absence of CH₄) can still be attributed to near
296 surface biological CO₂ production.

297 This 3 to 4% vol. CO₂ concentration range seems to be a threshold from which CH₄ oxidation
298 process has a significant influence onto CO₂ production whatever the sampling period
299 considered. At lower CO₂ concentrations, data are often lying in between the CH₄ oxidation
300 line and the replacement line. This indicates a mixed origin with part of the CO₂ deriving
301 from CH₄ oxidation and part of the CO₂ deriving from biological processes. The latter become
302 predominant for CO₂ concentrations lower than 2% vol. Such concentrations levels can

303 reasonably be assumed as the mean biological background concentrations (*e.g.* Gal *et al.*,
304 2014 and references therein). Nonetheless, Figure 4 outlines that even at such low CO₂
305 concentrations the influence of CH₄ oxidation process may exist thus suggesting a complex
306 behavior of gas emission towards the surface.

307 The CO₂ vs. O₂ plot allows the identification of another group of points that plots fairly well
308 on the replacement line (Figure 3A). Their CO₂ concentrations reach more than 5% vol. and
309 may represent soils with strong biological activity. Such concentrations are consistent with
310 concentrations up to 8-10% of biologically derived CO₂ reported in the literature (*e.g.* Gal *et*
311 *al.*, 2011, 2017b). These points are mainly located at the periphery of the monitoring zone
312 (black dots in Figure 3B). This may suggest the maximum extension of the methane-derived
313 CO₂-plume does not exceed a dozen of meters.

314 Figure 3

315

316 **4.3.2. O₂-N₂ relationship**

317 Processes are further constraint by O₂ vs. N₂ relationships (Romanak *et al.* 2012, 2017).
318 Figure 3C indicates the existence of two distinct behaviors, evidenced mainly by the 2015
319 data (only 6 measurements of the N₂ concentration in 2016). The slope of the regression fit
320 in green is close to -4 indicating quickly decreasing O₂ at near-constant, elevated N₂
321 concentrations. This corresponds to respiration processes and/or the presence of air as
322 defined by Romanak *et al.* (2012, 2017). O₂ depletion on this line may be linked to biological
323 processes, at least for O₂ concentration ranging from 21 down to 15-16% as suggested by
324 the CO₂-O₂ plot. At O₂ concentrations close to 15-16%, the gas analyses still indicate that no

325 CH₄ is associated with N₂, O₂ and CO₂. When O₂ concentrations are lower than 15%, then the
326 O₂ depletion becomes balanced by CH₄ and CO₂ concentrations increases (up to 12% and up
327 to 9% respectively). Points having constantly high N₂ concentrations are located in the
328 peripheral area surrounding the Fontaine Ardente main seep (black dots in the map; Figure
329 3C) where the influence of the gas seep becomes weaker. N₂ is only concerned by mixing
330 with seeping gases, whereas O₂ is consumed by oxidation of both organic matter in the
331 forest soil and of methane.

332 The second fit in Figure 3C (orange fit) has a slope of +0.265, close to the atmospheric O₂/N₂
333 ratio of 0.268, and represents the progressive mixing of air with N₂ and O₂ free gas vent
334 (dilution line). The corresponding points are in the vicinity of the main seep. This location
335 also well corresponds to points with a O₂ vs. CO₂ slope of ≥ 2 (Figure 3B) highlighting CH₄-
336 oxidation. Some data (7 points, yellow black circles in Figure 3C) fall between these two main
337 lines and they may correspond to some altered gas compositions. The spreading of these
338 data is influenced by the CH₄ content of the soil gas phase (points with the lower N₂
339 concentrations are the most enriched in CH₄, up to 74 %). These points are subject to a
340 variable influence of the gas vent with different rates of mixing between the geogenic and
341 the biological endmembers. Plotted on the map (Figure 3C), these data are located at the
342 peripheral of the gas vent highlighting the progressive – and non-linear – vanishing of the
343 geogenic gas input, progressively hidden by the biological gas production in soil.

344

345 **4.3.3. CO₂-CH₄ and O₂-CH₄ relationships**

346 As CO₂ and O₂ are closely linked, the relationships between CH₄ concentrations and CO₂ or
347 O₂ concentrations can be investigated in parallel (Figure 4). The CH₄ vs. O₂ relationship

348 shows less dispersion than the CH₄ vs. CO₂ relationship, as it is not affected by biological
349 production of CO₂ in soil that may alter the compositional ratios in between gas phases.

350 The linear fits indicated in black in Figure 4A and Figure 4B represent the influence of
351 atmospheric dilution. In the gas composition of the Fontaine Ardente main seep, no O₂ is
352 present and the CH₄ concentration is close to 90%. If air is present in the soil (*c.a.* 78% of N₂
353 and 21% of O₂) then a decrease of the CH₄ concentration by 10% is accompanied by an
354 increase of +2.1% in O₂ and of 7.8% in N₂ which corresponds to the atmospheric N₂/O₂ ratio.

355 The linear fits reported in blue in Figure 4A and Figure 4B correspond to rapid O₂ decrease
356 accompanied by CO₂ increase at near constant CH₄ with a slope close to -2.4. The underlying
357 process is oxidation of organic matter in the wood soil and root respiration, predominant in
358 points located at the periphery of the gas seep. Minor contribution of CH₄ oxidation to the
359 O₂ depletion and to the CO₂ enrichment may also exist. In the vicinity of the gas seep the
360 dominant process is the seepage of methane and associated CO₂.

361 Figure 4

362

363 **4.3.4. CO₂ flux – CH₄ flux relationship**

364 Figure 5 shows the relation between CO₂ and CH₄ fluxes. The Pearson's coefficient of
365 correlation, for the whole dataset, masks again a bimodal repartition of the data. Part of the
366 data shows a good linear fit between the two parameters but this relation is mainly defined
367 by a few high fluxes (3 data) whereas intermediate values are lacking (Figure 5A). In the
368 present case study, a CH₄ flux is considered as high when it is greater than 2 g/m²/h. Point 17
369 has a CH₄ to CO₂ flux ratio close to 1, compared to 2.1 and 2.4 for the two other points (28

370 and 31), whereas the ratios between CH₄ and CO₂ concentrations are respectively 6.1 (point
371 17), 9.4 (point 28) and 8.6 (point 31). In the lower CH₄ flux range (grey dots in Figure 5B) CH₄
372 flux represents approximately half of the CO₂ flux.

373 Two conclusions come from these statements. The first is that the emission of CH₄ is highly
374 variable over short distances albeit the higher fluxes are monitored in close vicinity to the
375 main seep. The second is that there is no relationship between the soil concentrations at 1 m
376 depth (Figure 4) and surface fluxes (Figure 5). This is a common observation in non-active
377 areas – no volcanic nor geothermal activity (*e.g.* Gal *et al.*, 2014). In areas of deep gas fluxes
378 (CO₂: *e.g.* Battani *et al.*, 2010; CH₄: *e.g.* Etiope *et al.*, 2011a) or where gas fluxes are
379 intentionally induced (*e.g.* Schroder *et al.*, 2016), the link with concentrations may be
380 stronger, even though complicated by transport through a thick soil column (*e.g.* Jones *et al.*,
381 2017).

382 The impervious geological substratum of the black shales would favor discrete gas flux on
383 fractures rather than diffuse fluxes. Another preferential pathway might be drillholes that
384 could have concentrated the formerly rather patchy gas leakage. At the surface level, the
385 combination of former reworking and the existence of a clayey cover may lead to poor
386 connection between CH₄ enrichment in the soil and CH₄ emission at the soil surface as the
387 driving force is not sufficient for allowing stronger efflux.

388 Numerous points in Figure 5B show low to very low CH₄ fluxes (less than 0.1 g/m²/h
389 excepted 1 sample at 0.18) and a wider scattering of the CO₂ flux (up to 4.5 g/m²/h). The
390 locations of these points are generally randomly distributed all around the gas seep with the
391 exception of some points (light blue and light blue-green dots in Figure 5B) which have CO₂
392 flux greater than 1 g/m²/h and which seem to surround the main seep a few meters away.

393 Even if the values of CH₄ fluxes are low, they are still influenced by the gas seep. Methane
394 emissions quantified in forests or in grasslands are indeed frequently 1000 times lower
395 (Jones *et al.*, 2005; Von Arnold *et al.*, 2005) and may rise up to 0.01 g/m²/h as a consequence
396 of agricultural practices such as cattle slurry spreading (Jones *et al.*, 2005) or in wetlands (Le
397 Mer and Roger, 2001). Similarly, CO₂ fluxes reaching 4.5 g/m²/h are still high compared to
398 fluxes measured in standard environments where they are generally 10 times lower with the
399 exception of agricultural spreading (up to 3.3 g/m²/h; Jones *et al.*, 2005) or enhanced
400 emissions in clayey soils (up to 2.3 g/m²/h; Gal *et al.*, 2014). The measured CH₄ and CO₂
401 fluxes are then still influenced by the existence of the gas seep but there is no clear relation
402 between the strength of the CO₂ flux and the location of the sampling point (Figure 5B). It is
403 then complicated to distinguish between a CO₂ flux mainly linked to the gas seep (CO₂
404 produced by CH₄ oxidation) and a variable contribution to the CO₂ flux of biological origin.

405 Figure 5

406

407 A few points showed a progressive depletion in oxygen concentration during the flux
408 measurement. These “negative” O₂ fluxes are reported in Figure 6 together with CO₂ and
409 CH₄ fluxes. Locations having the highest CO₂ and CH₄ flux (points 1, 17, 28, 31 and 73) plot on
410 linear fits thus suggesting that the O₂ depletion is intrinsically dependent from the strength
411 of the CH₄+CO₂ emission to the surface. Each rise of one flux unit is related to a decrease of
412 one unit of the O₂ flux with an intercept point at -3 to -4 g/m²/h, value under which the
413 accuracy of electrochemical sensing cells is not sufficient to allow adequate monitoring of
414 small changes of the O₂ concentration.

415 The most interesting case is point 73. At this location, the O₂ depletion is high (-10 g/m²/h),
416 the CO₂ flux is high (4.5 g/m²/h) and the CH₄ flux is zero. In the soil, there is an O₂ depletion
417 that is partially balanced by the presence of CO₂ (CO₂/O₂ = -1.5) and only traces of CH₄ are
418 found. The classical way for interpreting this O₂ depletion is to consider that an oxygen flux
419 from the atmosphere to the soil exists. Nevertheless, point 73 plots on the CO₂ flux – O₂ flux
420 linear fit that is defined for locations where a CH₄ flux exists. The O₂ depletion monitored at
421 this point thus represents the influence of the CH₄ gas seep and the genesis of O₂ depletion
422 is a consequence of CH₄ oxidation that produces CO₂ that is to some extent mixed with
423 biologically produced CO₂.

424 Figure 6

425

426 **4.4. Data analysis**

427 **4.4.1. Qualifying and quantifying the CH₄ and related CO₂ emissions at the**

428 **Fontaine Ardente (main seep and peripheral areas)**

429 **4.4.1.1. Variability of the gas emissions**

430 The variability of soil gas signals can be considered along three different time scales from
431 short variations to daily variations and yearly changes. During the two field surveys, no
432 strong daily variations of the soil gas signals were observed. This may be a consequence of
433 the restricted emissive area. Similarly, between the two surveys, the gas anomalies in the
434 soil had the same order of magnitude suggesting that the contrasting meteorological
435 conditions in 2015 and in 2016 had little influence. Over longer time scales, Etiope *et al.*
436 (2010) have highlighted thermal forcing on flux emissions in a gas seep in Switzerland but

437 they also established that air pressure and relative humidity have no influence onto long-
438 term measurements.

439 The other time scale that can be considered is the 3 min duration of flux integration during
440 chamber measurements. Gas emission of major species can also be variable over few
441 minutes (Figure 7). Point 10 represents the routine situation with linear increase of the CO₂
442 concentration indicating constant gas emission. The situation was different for some
443 monitoring points. Examples of varying flow are shown for points located close to the gas
444 seep (Figure 7). We observe both examples of sudden and simultaneous increases of CO₂
445 and CH₄ fluxes (point 13) and decreases (points 15 and 17) that are not necessarily
446 synchronous for both gases (point 17). Very short-term changes have also been observed
447 (point 17). These variations may induce a bias in the estimation of fluxes. Of 69 CO₂ and 54
448 CH₄ flux measurements, respectively 17 and 12 showed variations, and for two in each case
449 fluxes were potentially underestimated.

450 We could not perform repeated monitoring at these points so the bias linked to these short
451 to very short term fluctuations of the seepage rate could not be precisely assessed. These
452 fluctuations are also attested by the rapidly changing height of the flame as depicted
453 in Figure 8. An estimation of the bias that may be related to this short term variability has
454 been done by examining each gas accumulation curve during time. On the 69 CO₂ flux
455 measurements, 17 showed temporal variation during the CO₂ accumulation phase among
456 which only 2 were potentially underestimated. On the 56 CH₄ flux measurements, 12
457 showed temporal variation and by them 2 were also potentially underestimated. Thus, the
458 flux measurements may rather lead to a slight overestimation of the global CO₂ and CH₄
459 budgets released into the atmosphere so that our estimates can be considered conservative.

460 Figure 7

461 Figure 8

462

463 **4.4.1.2. Spatial distribution**

464 Albeit our dataset is relatively limited compared to those that may be used e.g. in volcanic
465 environments (*e.g.* Ciotoli *et al.*, 2016), such investigations on small areas can nevertheless
466 yield to accurate estimates of both the gas emissions and the pattern of these emissions
467 (Etiopie *et al.*, 2010). As may be viewed from data available in the supplementary
468 information, our dataset is skewed and neither ranges under normal nor log-normal data
469 distributions. The existing bimodal distribution is a consequence of the existence of two
470 distinct phenomena. The first is the presence of the gas seep and the second are common
471 biological processes in soils. The definition of threshold values is thus done using quantile-
472 quantile (Q-Q) plots (*e.g.* Ciotoli *et al.*, 2007) further allowing the calculation of the quantity
473 of gas emitted to the atmosphere using Graphical Statistical Analysis (*e.g.* Bloomberg *et al.*,
474 2012, and references therein).

475 Variogram calculations were done for the data falling in the 20x20 m side square around the
476 main seep (see supplementary information). All the data show an anisotropic pattern with
477 the main axis elongated along the N45 direction with a length ranging from 6.5 to 13.7 m
478 (9.2 m as a mean). Such a shape is in good agreement with the spatial extent of the gas vent
479 that may be deduced directly from field measurements: high CH₄ values were found along
480 the axis of the Vernant creek which flows to the NE and these high values were found in a
481 narrow perimeter (less than 20 m of side).

482 Data are used to build classed post maps (shown in supplementary information) and
483 interpolated maps (Figure 9). Classed post maps are presented for the entire monitoring
484 area with detail for the vicinity of the main seep whereas contours maps only refer to this
485 area of reduced size. These maps highlight once again that the majority of soil gas anomalies
486 are located within few meters around the gas seep. From the classed post maps it is not
487 obvious to define whether the degassing is structured along pathways inherited from
488 structural or morphological features or if the degassing occurs randomly close to the vent.

489 A better definition of the spatial distribution of the degassing processes is given by contour
490 maps (Figure 9). The N45 direction, which is the average flow direction of the Vernant creek
491 and which was also highlighted by variogram calculations, suggests the existence of
492 preferential pathways inherited from structural constraints. A second direction of degassing
493 can also be defined using the helium gas contents in soil probably related to the ability of
494 helium to laterally diffuse as a consequence of its low molecular weight (*e.g.* Toutain and
495 Baubron, 1999). This second direction is close to N170, a direction that is commonly found in
496 the limestones of the Vercors Massif. As for classed post maps, flux data do not allow
497 defining or refining the structural shape of the gas emissions to the surface. Contour maps
498 are dominated by a few outliers (high fluxes) which induce a peak-like interpolation. This
499 may be a consequence of site alterations in the since the 19th century: the point where CO₂
500 and CH₄ emissions to the atmosphere are at their maximum value is indeed located on a
501 break of slope, in front of the gabion wall that has been built to shelter the fountain, as
502 visible on Figure 1 in the foreground of the panoramic photo.

503 Figure 9

504

505

506

4.4.1.3. Gas emissions to the atmosphere

507 Even if the Fontaine Ardente gas seep has a rather limited spatial extension – other seeps
508 may have considerably larger geographical manifestations (*e.g.* Etiope *et al.*, 2011b) – the
509 evaluation of the CH₄ and CO₂ emissions to the atmosphere is interesting. As shown by the
510 site monitoring, the main emission point is clearly the main seep itself, probably in strong
511 relation with the existence of the former FA2 borehole (Figure 1) that focuses the gas
512 emission by draining. Nonetheless, gas fluxes to the atmosphere are not restricted to the
513 former borehole and exist over a larger area that extends northeastwards from the seep and
514 their contribution has also to be quantified.

515 Estimations on the gas release at the seep mouth are done using the fire dynamics model of
516 methane flux vs. flame size (Etiope *et al.*, 2011b, and references therein) using the heat of
517 combustion given by Etiope *et al.* (2013a) for CH₄. Typology of the gas emission is taken from
518 flame height and diameter at emission point estimated using Figure 8. As the main seep
519 exhibits rapid changes in the flame height, the emission rate ranges between 15 kg per day
520 (flame of 38 cm height and 12 cm on diameter) and 84 kg per day (flame of 77 cm height and
521 24 cm on diameter). Based on the flame size variations that may be observed at the seep at
522 short time scale, the amount of CH₄ released in the atmosphere can be estimated to be
523 somewhere between 40 and 50 kg per day. The estimated release rate in the 90's, obtained
524 from pressure considerations (Berthier *et al.*, 1991), was 130 l/min giving approx. 120 kg of
525 CH₄ per day. Our present estimates, based on the flame height, may then be underestimated
526 *e.g.* as a consequence of short duration of the measurements. A significant uncertainty on
527 the result has been pointed out by Etiope *et al.* (2011b) especially when the gas emission is

528 high and turbulent. This new estimate may also represent a real decrease in the feeding rate
529 of the borehole, the gas flux migrating along this preferential pathway changing with time.

530 The case of the Fontaine Ardente degassing area is also interesting insofar as this gas seep is
531 CO₂-rich. Using the CH₄ flux estimated in the 90's and the proportion of CO₂ in the gas phase
532 (approx. 11%), the quantity of CO₂ released in the atmosphere through the vent can be
533 roughly estimated at 14 l/min *i.e.* 36 kg per day. Based on flame height estimates and still
534 considering a proportion of CO₂ in the gas phase of 11%, then the estimate of the CO₂
535 release at the gas vent is close to 15 kg per day as a mean (range: 4.5 to 25 kg per day).

536 The CH₄ and CO₂ emissions from the soil are first quantified on a 84 m² area included in the
537 larger 20 x 20 m area reported on Figure 9. The area is not a square area as the vicinity of
538 the gas seep cannot be investigated (concrete plugs + gabion) but its geometry is likely to be
539 representative as most of the efflux is located inside this small region (see Figure 9). This
540 approach considers that the flux measured at one point is valid for 1 m²; in case the grid
541 mesh is 2 x 1 m, then the value assigned in between two real measurements is the mean
542 value of these two measurements. The sum of the fluxes is 44.8 g/h for CH₄ and 88.3 g/h for
543 CO₂ leading to releases of 1.07 kg of CH₄ and 2.2 kg of CO₂ per day. A refined estimate is
544 obtained using the interpolated maps. Integration of the anomaly is done using Surfer®
545 software and indicates, for the whole flux monitoring zone (240 m²; Figure 9), a release of
546 2.83 kg of CH₄ and 6.27 kg of CO₂ per day. These estimates are in perfect agreement with
547 those obtained using the 84 m² area [$1.07 \times (240/84) = 3.05$] suggesting that even the basic
548 method could lead to realistic evaluation in the present case. Nonetheless this flux estimate
549 doesn't take into account gas emissions that may occur with the area covered by concrete
550 plugs which may be fissured and permeable to gas.

551 More sophisticated methods (*e.g.* Bloomberg *et al.*, 2012) or other spatial interpolation
552 methods (*e.g.* Schroder *et al.*, 2017) may be used to quantify more precisely the leakage
553 associated to the gas seep. Nonetheless, even well constrained data interpolation methods
554 lead to biases in the emission estimates. During controlled release experiments, Schroder *et*
555 *al.* (2017) report differences of 20 to 45% using the method that best fits the data. In the
556 present case, the main emission is the gas seep itself, and errors on the soil emissions may
557 be considered as negligible. Methane emission at gas vent ranges from 18 to 44 tons per
558 year (2016 flame estimate / 1990 data) and CO₂ emission ranges from 5.5 to 13 tons per
559 year. Referring to our measurements, the CH₄ emission from soils represents less than 6% of
560 the CH₄ emitted at the seep (1.03 ton per year) whereas the CO₂ emission from soils
561 accounts for 42% of the CO₂ emitted at the seep (2.3 tons per year) including biogenic soil
562 CO₂. This biological component can be estimated to account for two thirds of the CO₂ release
563 on the basis of volumes calculated using interpolated maps with a biological CO₂ production
564 fixed at 1.25 g.m⁻².h⁻¹ (Werner and Brantley, 2003).

565 Conjoint emission of CH₄ and CO₂ in gas seep is not a common phenomenon. In the
566 European database from Etiope *et al.* (2009) or the data from other countries (Etiope *et al.*,
567 2011a), which concern mud volcanoes, CO₂-rich emissions (8% vol. or more) are rare and
568 linked to thermogenic CH₄. CH₄ seep rates associated to mini- and micro-seepages range
569 from less than 10 up to 446 g/m²/day; associated CO₂ seep rates range from 3 to 535
570 g/m²/day (Etiope and Klusman, 2002). Maximum seep rates measured at point 17 are in this
571 range (408 and 374 g/m²/day for CH₄ and CO₂ resp.). Abiotic methane emissions from
572 ultrabasic rocks are associated with very low CO₂ emissions (Etiope *et al.*, 2011b). In such
573 cases, CH₄ emissions can reach hundreds of g per day per m² but CO₂ emissions only reach
574 65 g/m²/day when soil litter is present and 10 g/m²/day when soil is absent. Eternal flames

575 from the USA (Etiope *et al.*, 2013a) or gas seeps reported in Switzerland (Etiope *et al.*, 2010)
576 are not reported to be CO₂-rich but CH₄ emissions can reach 40 kg per day and 10 kg per day
577 respectively in the US and in Switzerland (strong miniseepages, from hundreds of g/m²/day
578 up to a few kg/m²/day). Similarly, studies of the large thermogenic gas seepage of Katakolo
579 (Greece) only report CH₄ emissions (from 5.4 to 98.6 kg per day onshore; Etiope *et al.*,
580 2013b) albeit 6 to 8% vol. of CO₂ are monitored in the gas phase. Quantification of CO₂
581 emissions from natural methane seeps is rare, opposite to numerous studies of CO₂
582 emissions in volcanic or geothermal areas (*e.g.* Cardinelli *et al.*, 2003b).

583 The Fontaine Ardente area has thus a specific behavior that may partly be a consequence of
584 the presence of a draining structure (borehole) and related impact onto surface properties
585 of soil. Methane is found at high concentrations in the soil with moderate to weak leakage
586 into the atmosphere. Most of the CH₄ is vented through the borehole that constitutes by
587 itself an important gas seep. According to the terminology of Etiope (2015), miniseepage
588 occurs around the gas vent but only accounts for 5% of the global budget of CH₄ emitted
589 (compared to the lowest estimate of 18 tons/y). This differs from the gas emission reported
590 in the Giswil by Etiope *et al.* (2010) where two thirds of the CH₄ are vented through two
591 main seeps and one third is vented by miniseepage on a smaller area (115 m² compared to
592 240 m² at Fontaine Ardente area). The other specific character of the Fontaine Ardente
593 seepage area is the richness of the gas phase in CO₂. At the scale of the miniseepage area,
594 this leads to a quantity of CO₂ emitted being more than two times that of CH₄. This is a
595 rather unique situation in the Alpine context and GHG emissions evaluations have to
596 considerer both CH₄ and CO₂ gas phases to be pertinent.

597 The other specificity of the Fontaine Ardente main seep is that it represents a unique
598 analogue of a leakage situation. Hydrocarbon resources are rarely located at few meters
599 below ground level. Here, a borehole intersects at c.a. 10 m depth geological formations
600 which act as drain for CH₄+CO₂ gas mixture. The borehole as preferential pathway focuses
601 gas emissions to the surface, similarly to degassing pipes like those in lakes Nyos and
602 Monoun (Halbwachs *et al.*, 2004). The gas which is not vented through the borehole diffuses
603 laterally in the subsurface layers through pathways whose geometry is likely to be influenced
604 by the network of local fractures.

605 Old pictures, previous to drilling, clearly show numerous small vents, whereas at present
606 there is a unique and dominant gas seep with only minor contribution of diffuse seepage.
607 This highlights the impacts of small-scale works on gas flux patterns.

608

609 **5. Implications for methane or CO₂ baseline assessment and monitoring**

610 Several tens of tons per year of both CH₄ and CO₂ gas phases are naturally released in the
611 atmosphere by the Fontaine Ardente main seep thus contributing to GHG emissions over at
612 least two millenaries. Apart from gas released at the borehole mouth, the amounts of CO₂
613 emitted through soil degassing may largely exceed the range of natural CO₂ flux (from 7.6 to
614 76 g/m²/day; Klusman, 2015, and references therein) with maximum values greater than 350
615 g/m²/day. Similarly, CH₄ emissions reaching 10 g per m² per day around the main seep are
616 considerably higher than those measured over grasslands during summertime with
617 4.86±22.8 mg per m² per day (mean + standard deviation) reported by Klusman (2015, and
618 references therein). Apart from this quantification of GHG emissions, a second interest of
619 this study was to test monitoring techniques and strategies to better assess the natural gas

620 baseline for impact studies. The production of unconventional natural gas has profoundly
621 transformed the global energy game over the past ten years. Environmental stakes of shale
622 gas exploration and exploitation show some similarities with the CCS thematic, specifically
623 with the risk of leakage from geological formations from which CH₄ can be produced or in
624 which CO₂ can be stored, albeit the gas species of interest have very different behavior in
625 *e.g.* their reactivity or dissolution properties.

626 The example of the Fontaine Ardente seepage area makes it possible to investigate
627 simultaneously methane and CO₂ migration on a unique natural analogue and to learn more
628 about containment monitoring in settings where potential pathways to the surface exist
629 (Jenkins *et al.*, 2015). It constitutes furthermore one of the rare examples of “eternal flames”
630 directly emerging from shale formations, together with those from the Appalachians (Etiope
631 *et al.*, 2013). More specifically, the Fontaine Ardente main seep case represents an example
632 where the leakage is focused to a 1D pathway, represented by the former FA2 borehole.
633 Here, the leakage does not occur from the casing itself, because of the presence of a
634 concrete platform at surface, or from defective completion of the casing, which will be the
635 most frequent occurrence of failure. Leakage occurs through the open borehole and this
636 drillhole has strongly modified the gas emission on the site. From a spotty and rather diffuse
637 leakage situation, attested by old photographs, it has been changed to a gas vent, with the
638 borehole as main emitting structure, with minor contribution of diffuse degassing. It is thus
639 possible that a hypothetical closure of the well will induce a highly different distribution of
640 the seepage with strongly enhanced diffuse degassing, probably occur along fractures/faults
641 following the main structural directions (Roberts *et al.*, 2015; Bond *et al.*, 2017).

642 This natural analogue highlights the potential difficulties of baseline assessment and site
643 monitoring during exploration or exploitation of unconventional gas. The expected spatial
644 extension of the leakage will condition the resolution of the monitoring grid (e.g.
645 observation boreholes) and wrong initial hypotheses may lead to an incapacity to detect any
646 anomaly related to leakage. The strongly focused fluxes at the Fontaine Ardente seepage
647 area, further enhanced by the drilling, are somewhat similar to what might be expected in
648 case of shale gas well failure, with a very restricted area of leakage around the borehole.
649 Other leakage pathways, e.g. out-of-formation hydraulic fracturation, may lead to a much
650 more diffuse pattern at surface, due to the predominantly diffusive or pervasive migration,
651 from the host formation, via overlying deep aquifers to shallow formations. Timing of such
652 migration can be also very different from direct pathways via leaking wells.

653 Transposed to a real shale gas or CCS site, the difficulty to anticipate and detect gas seepage
654 areas will be a major challenge for baseline assessment and site monitoring. The area
655 studied here is very small (around 240 m²), vegetated and set in a narrow thalweg. Surveying
656 methods used directly at ground level may not be operative (too large mesh size) or they
657 should require so much manpower that their cost will dramatically increase in case the grid
658 has a very low mesh size. There is an extensive literature that points out the narrowness of
659 gas emissions from faults and fractures and very recent data still agree with this feature (e.g.
660 Jolie *et al.*, 2016; Bond *et al.*, 2017). The disadvantage of ground monitoring techniques may
661 be overcome by airborne/UAV operated methods or methods having wider aperture (such
662 as Eddy-Covariance – EC, laser operated methods...). Such methods are capable of giving
663 better geographical coverage provided that they are appropriately settled. In the case of the
664 EC method, changes of gas flux are monitored in an upwind direction. Nevertheless such
665 methods may suffer from other disadvantages such as the decrease in sensitivity as a

666 function of distance to the emission point or the existence of photosynthetic processes on
667 land surface or in the canopy (Klusman, 2015).

668 When working in a blind manner during baseline studies, in a setting similar to that of
669 Fontaine Ardente area, it seems very difficult to detect gas anomalies related to minor or
670 even major gas seeps. Topography and vegetation play an important role in the detectability
671 of anomalies. Natural seeps from shale formations, as it is the case for the Fontaine Ardente,
672 are frequently located on creeks, themselves following fault structures (Etiopie *et al.*, 2013a).
673 Their detectability by landborne methods may be simply limited by logistic obstacles and
674 sampling resolution. With the available techniques, it seems virtually impossible to discover
675 unknown seeps through a systematic research. Etiopie *et al.*, (2013a) used the Tunable Diode
676 Laser Absorption Spectroscopy (TDLAS) detectors in accumulation flux chambers to locate
677 methane anomalies in ambient air but only in the vicinity of known eternal flames. Using a
678 statistically stringent measurement pattern (grid) for landborne surveys would be hindered
679 by (1) the accessibility of natural areas with rough terrain and (2) the possible resolution of
680 such a grid compared to the size of anomalies. Some hope can be placed in vehicle-born
681 surveys using CRDS (Cavity Ring-Down Spectroscopy) detectors but this approach fits best to
682 urban areas with a high road density (Gallagher *et al.*, 2015) as well as to anthropogenic
683 sources identified previously to the survey (Zazzeri *et al.*, 2015). It is unlikely that natural
684 point-source emissions from gas seeps of a similar size to the Fontaine Ardente could be
685 detected by such a technique. Airborne techniques, again using CRDS, are capable of
686 detecting major methane plumes from known sources (e.g. landfills; Krautwurst *et al.*, 2017)
687 at kilometeric scale but, again, their use in the present case seems to be highly limited by the
688 vegetation cover and the topography.

689 To approximatively assess the vertical extension of the plume emitted by the Fontaine
690 Ardente we used infrared cameras with specific lenses for targeting CH₄ or CO₂ gas phases
691 (FLIR GF320). Such devices can image the gas plume emitted by the borehole and its
692 dispersal in the atmosphere. Some wisps of gas do reach the base of the canopy, some
693 meters above ground level, but they rather rapidly vanish afterwards (Figure 10). If the
694 leakage flux rate is lower than the one of the Fontaine Ardente main seep (FA2 borehole),
695 the detection by plume imaging becomes virtually impossible in practice. Thorough scanning
696 of the miniseepage area did allow detecting a possible leakage area only after minutes of
697 careful monitoring. It is established that such infrared cameras are not conceived for the
698 detection of diffuse minor leaks in a natural environment (contrast problems) and that other
699 monitoring techniques have considerably lower detection limits. Nevertheless, such cameras
700 allow visualizing in real time the shape of the gas emissions especially vertically. Given our
701 preliminary results, any other monitoring at the upper level of the canopy will be very
702 difficult even using techniques with low detection ranges, including low-altitude airborne
703 techniques.

704 Figure 10

705

706 The question on the best baseline and monitoring strategy for leakage assessment remains
707 thus largely open. Landborne monitoring will always miss anomalies because of restricted
708 accessibility – in our case the ability to perform accurate measurement in forested area – or
709 because of lack of sensitivity – in our case quick dilution of the gas in the atmosphere.
710 Consequently, appropriate monitoring strategy should rely on dense monitoring of
711 structures and/or areas that are suspected to be potential pathways for leakage (known

712 faults, creeks...; Etiope *et al.*, 2013a). As dense monitoring cannot cover a large area,
713 monitoring should be adapted to the size and location of the expected leak. This requires a
714 realistic conceptual model of the leakage mechanisms and pathways, relying on a
715 statistically sound database of gas emissions in the context of the storage to monitor. The
716 temporal resolution of monitoring and its duration is another crucial issue, depending on (1)
717 the temporal variations of the baseline emissions and (2) the kinetics of potential gas
718 migration via the different suspected pathways (e.g. borehole failures, out-of-formation
719 fracturation..., existence natural fractured zones). In case of leakage allegation, even if the
720 alleged zone has not been surveyed before, the knowledge of local behavior of soil gas
721 emissions will allow to adequately identify an anomaly in the soil gas signals – an approach
722 defined as process-based approach by Romanak *et al.* (2012). The example on how the
723 leakage allegation in Weyburn was withdrawn shows how powerful such an approach can
724 be. Furthermore, it may not only apply to soil gas using the established CO₂ vs. O₂
725 relationship but also to soil gas fluxes using the derivative relation CO₂ flux vs. O₂ depletion is
726 the soil efflux.

727 **Acknowledgments**

728 This research was conducted in the frame of the G-baseline project, co-funded by the French
729 Research Agency (ANR-14-CE05-0050 grant) and the Natural Sciences and Engineering
730 Research Council of Canada (NSERC grant n° 463605).

731 The representative of FLIR Systems France (Stéphane Thiebaut) is thanked for the
732 demonstration of infrared cameras.

733 **References**

734 Armannsson H., Fridriksson T., Kristjansson B.R., 2005, CO₂ emissions from geothermal
735 power plants and natural geothermal activity in Iceland, *Geothermics* 34, 286-296.

736 Association Histoire et Patrimoine du Gua (AHPG), 2012, La Fontaine Ardente, merveille du
737 Dauphiné, "Histoire et Patrimoine du Gua" Eds., 68 p.

738 Battani A., Deville E., Faure J.-L., Noirez S., Tocqué E., Jeandel E., Benoît Y., Schmitz J.,
739 Parlouar D., Gal F., Le Pierrès K., Brach M., Braibant G., Bény C., Pokryszka Z., Charmoille A.,
740 Bentivegna G., Pironon J., de Donato P., Garnier C., Cailteau C., Barrès O., Radilla G., Bauer
741 A., 2010, Geochemical study of the natural CO₂ emissions in the French Massif Central: How
742 to predict origin, processes and evolution of CO₂ leakage, *OGST*, 65(4), 615-633.

743 Baxter P.J., Baubron J.-C., Coutinho R., 1999, Health hazards and disaster potential of ground
744 gas emissions at Furnas volcano, Sao Miguel, Azores, *Journal of Volcanology and Geothermal*
745 *Research* 92, 95-106.

746 Berthier M., Honegger J.L., Eberentz P., 1991, Etude et travaux pour le renforcement en gaz
747 de la Fontaine Ardente - Commune du Gua (Isère), BRGM report R-33584-RHA-4S/91, 38 p.

748 Bloomberg S., Rissmann C., Mazot A., Oze C., Horton T., Gravley D., Kennedy B., Werner C.,
749 Christenson B., Pawson J., 2012, Soil gas flux exploration at the Rotokawa geothermal field
750 and White Island, New Zealand, Proceedings of the 36th Workshop on Geothermal Reservoir
751 Engineering, Stanford University, Stanford, California, January 30 – February 1, 2012.

752 Bond C.E., Kremer Y., Johnson G., Hicks N., Lister R., Jones D.G., Haszeldine R.S., Saunders I.,
753 Gilfillan S.M.V., Shipton Z.K., Pearce J., 2017, The physical characteristics of a CO₂ seeping

754 fault: The implications of fracture permeability for carbon capture and storage integrity,
755 *International Journal of Greenhouse Gas Control* 60, 49-60.

756 Bouma T.J., Bryla D.R., 2000, On the assessment of root and soil respiration for soils of
757 different textures: interactions with soil moisture contents and soil CO₂ concentrations,
758 *Plant and Soil*, 227, 215-221.

759 Brantley S.L., Koepenick K.W., 1995, Measured carbon dioxide emissions from Oldoinyo
760 Lengai and the skewed distribution of passive volcanic fluxes, *Geology*, vol. 23, No 10, 933-
761 936.

762 Capaccioni B., Martini M., Mangani F., Giannini L., Nappi G., Prati F., 1993, Light
763 hydrocarbons in gas-emissions from geothermal fields volcanic areas and geothermal fields,
764 *Geochemical Journal* Vol. 27, 7-17.

765 Chiodini G., Cioni R., Guidi M., Raco B., Marini L., 1998, Soil CO₂ flux measurements in
766 volcanic and geothermal areas, *Applied Geochemistry*, 13(5), 543-552.

767 Ciotoli G., Lombardi S., Annunziatellis A., 2007, Geostatistical analysis of soil gas data in a
768 high seismic intermontane basin: Fucino Plain, central Italy, *Journal of Geophysical Research*,
769 112, B05407.

770 Ciotoli G., Etiope G., Marra F., Florindo F., Giraudi C., Ruggiero L., 2016, Tiber delta CO₂-CH₄
771 degassing: A possible hybrid, tectonically active Sediment-Hosted Geothermal System near
772 Rome. *Journal of Geophysical Research: Solid Earth*, 121(1), 48-69.

773 D'Alessandro W., Yüce G., Italiano F., Bellomo S., Gülbay A.H., Yasin D.U., Gagliano A.L.,
774 2018, Large compositional differences in the gases released from the Kizildag ophiolitic body

- 775 (Turkey): Evidences of prevailingly abiogenic origin, *Marine and Petroleum Geology*, [89](#), 174-
776 [184](#).
- 777 Durand M., Scott B.J., 2005, Geothermal ground gas emissions and indoor air pollution in
778 Rotorua, New Zealand, *Science of the Total Environment* 345, 69-80.
- 779 Etiope G., Klusman R.W., 2002, Geologic emissions of methane to the atmosphere,
780 *Chemosphere*, 49, 777-789.
- 781 Etiope G., Martinelli G., 2002, Migration of carrier and trace gases in the geosphere: an
782 overview, *Physics of the Earth and Planetary Interiors* 129, 185-204.
- 783 Etiope G., 2009, Natural emissions of methane from geological seepage in Europe,
784 *Atmospheric Environment*, 43, 1430-1443.
- 785 Etiope G., Feyzullayev A., Milkov A.V., Waseda A., Mizobe K., Sun C.H., 2009, Evidence of
786 subsurface anaerobic biodegradation of hydrocarbons and potential secondary
787 methanogenesis in terrestrial mud volcanoes, *Marine and Petroleum Geology*, 26, 1692-
788 1703.
- 789 Etiope G., Zwahlen C., Anselmetti F.S., Kipfer R., Schubert C.J., 2010, Origin and flux of a gas
790 seep in the Northern Alps (Giswil, Switzerland), *Geofluids*, 10, 476-485.
- 791 Etiope G., Nakada R., Tanaka K., Yoshida N., 2011a, Gas seepage from Tokamachi mud
792 volcanoes, onshore Niigata Basin (Japan): Origin, post-genetic alterations and CH₄-CO₂
793 fluxes, *Applied Geochemistry*, 26, 348-359.

- 794 Etiope G., Schoell M., Hosgörmez H., 2011b, Abiotic methane flux from the Chimaera seep
795 and Tekirova ophiolites (Turkey): Understanding gas exhalation from low temperature
796 serpentinization and implications for Mars, *Earth and Planetary Science Letters*, 310, 96-104.
- 797 Etiope G., Drobniak A., Schimmelmann A., 2013a, Natural seepage of shale gas and the origin
798 of “eternal flames” in the Northern Appalachian Basin, USA, *Marine and Petroleum Geology*,
799 43, 178-186.
- 800 Etiope G., Christodoulou D., Kordella S., Marinaro G., Papatheodorou G., 2013b, Offshore
801 and onshore seepage of thermogenic gas at Katakolo Bay (Western Greece), *Chemical*
802 *Geology*, 339, 115-126.
- 803 Etiope G., 2015, Natural Gas Seepage, The Earth’s Hydrocarbon Degassing, Springer.
- 804 Etiope G., 2017, Abiotic methane in continental serpentinization sites: an overview, 15th
805 Water-Rock Interaction International Symposium, WRI-15, *Procedia Earth and Planetary*
806 *Science* 17, 9-12.
- 807 Fridriksson T., Kristjansson B.R., Armannsson H., Margretardottir E., Olafsdottir S., Chiodini
808 G., 2006, CO₂ emissions and heat flow through soil, fumaroles, and steam heated mud pools
809 at the Reykjanes geothermal area, SW Iceland, *Applied Geochemistry*, 21, 1551-1569.
- 810 Gal F., Joubin F., Haas H., Jean-Prost V., Ruffier V., 2011, Soil gas (²²²Rn, CO₂, ⁴He) behaviour
811 over a natural CO₂ accumulation, Montmiral area (Drôme, France): geographical, geological
812 and temporal relationships, *J. Env. Rad.*, 102, 107-118.
- 813 Gal F., Michel K., Pokryszka Z., Lafortune S., Garcia B., Rouchon V., de Donato P., Pironon J.,
814 Barrès O., Taquet N., Prinnet C., Hy-Billiot J., Lescanne M., Cellier P., Lucas H., Gibert F., 2014,
815 The SENTINELLE French research project: subsurface geochemical characterization prior CO₂

816 injection (baseline survey) - site of Rouse (TOTAL CCS Pilot), *International Journal of*
817 *Greenhouse Gas Control*, 21, 177-190.

818 Gal F., Kloppmann W., Proust E., Bentivegna G., Defossez P., Mayer B., Gaucher E.C., 2017a,
819 Natural CH₄ gas seeps in the French Alps: characteristics, typology and contribution to CH₄
820 natural emissions to the atmosphere, *Energy Procedia*, 114, 3020-3032.

821 Gal F., Proust E., Bentivegna G., Leconte S., De Lary De Latour L., Loschetter A., Pokryszka Z.,
822 Collignan B., 2017b, What may be the consequences of a CO₂ leakage? Insights from soil gas
823 measurements in an urban area – Clermont-Ferrand, French Massif Central, *Energy Procedia*,
824 114, 3006-3019.

825 Gallagher M.E., Down A., Ackley R.C., Zhao K.G., Phillips N., Jackson R.B., 2015, Natural Gas
826 Pipeline Replacement Programs Reduce Methane Leaks and Improve Consumer Safety,
827 *Environmental Science & Technology Letters* 2, 286-291.

828 Greenland L.P., Rose W.I., Stokes J.B., 1985, An estimate of gas emissions and magmatic gas
829 content from Kilauea volcano, *Geochimica et Cosmochimica Acta*, Volume 49, Issue 1, 125-
830 129.

831 Halbwachs M., Sabroux J.C., Grangeon J., Kayser G., Tochon-Danguy J. C., Felix A., Béard J.C.,
832 Villevieille A., Vitter G., Richon P., Wüest A., Hell J., 2004, Degassing the “killer lakes” Nyos
833 and Monoun, Cameroon, *EOS, Transactions, American Geophysical Union*, Vol. 85, No 30,
834 281-285.

835 Halmer M.M., Schmincke H.-U., Graf H.-F., 2002, The annual volcanic gas input into the
836 atmosphere, in particular into the stratosphere: a global data set for the past 100 years,
837 *Journal of Volcanology and Geothermal Research* 115, 511-528.

- 838 Hinkle M.E., 1994, Environmental conditions affecting concentrations of He, CO₂, O₂ and N₂
839 in soil gases, *Applied Geochemistry*, 9, 53-63.
- 840 Hobbs P.V., Radke L.F., Lyons J.H., Ferek R.J., Coffman D.J., Casadevall T.J., 1991, Airborne
841 measurements of particle and gas emissions from the 1990 volcanic eruptions of Mount
842 Redoubt, *Journal of Geophysical Research*, vol. 96, No D10, 18,735-18,752.
- 843 Holloway S., Pearce J.M., Hards V.L., Ohsumi T., Gale J., 2007, Natural emissions of CO₂ from
844 the geosphere and their bearing on the geological storage of carbon dioxide, *Energy* 32,
845 1194-1201.
- 846 Humez, P., Mayer, B., Nightingale, M., Becker, V., Kingston, A., Taylor, S., Bayegnak, G.,
847 Millot, R., Kloppmann, W., 2016. Redox controls on methane formation, migration and fate
848 in shallow aquifers. *Hydrology and Earth System Sciences* 20, 2759–2777.
- 849 Jenkins C., Chadwick A., Hovorka S.D., 2015, The state of the art in monitoring and
850 verification—Ten years on, *International Journal of Greenhouse Gas Control* 40, 312-349.
- 851 Jolie E., Klinkmueller M., Moeck I., Bruhn D., 2016, Linking gas fluxes at Earth's surface with
852 fracture zones in an active geothermal field, *Geology*, Vol. 44, No. 3, 187-190.
- 853 Jones S.K., Ress R.M., Skiba U.M., Ball B.C., 2005, Greenhouse gas emissions from a managed
854 grassland, *Global Planet. Change*, 47, 201-211.
- 855 Jones D.G., Beaubien S.E., Lister T.R., Graziani S., Finioia M.G., Barkwith A.K.A.P., Ruggiero L.,
856 Ciotoli G., Bigi S., Lombardi S., 2017, Continuous monitoring of natural CO₂ emissions near
857 Rome – lessons for low-level CO₂ leakage detection, *Energy Procedia*, 114, 3824-3831.

- 858 Kloppmann W., Blessing M., Proust E., Gal F., Bentivegna G., Henry B., Defossez P., Catherine
859 C., Humez P., Mayer B., Millot R., Gaucher E.C., 2016, Natural gas seeps in the French Alps:
860 Sources and pathways, *Geophysical Research Abstracts*, 18, pp. EGU2016-14484, EGU2016.
- 861 Klusman R.W., 2015, Surface geochemical measurements applied to monitoring, verification,
862 and accounting of leakage from sequestration projects, *Interpretation*, Vol. 3, No. 2, p. SM1–
863 SM21, <http://dx.doi.org/10.1190/INT-2014-0093.1>.
- 864 Krautwurst S., Gerilowski K., Jonsson H.H., Thompson D.R., Kolyer R.W., Iraci L.T., Thorpe
865 A.K., Horstjann M., Eastwood M., Leifer I., Vigil S.A., Krings T., Borchardt J., Buchwitz M.,
866 Fladeland M.M., Burrows J.P., Bovensmann H., 2017, Methane emissions from a Californian
867 landfill, determined from airborne remote sensing and in situ measurements, *Atmospheric*
868 *Measurement Techniques* 10, 3429-3452.
- 869 Le Mer J., Roger P., 2001, Production, oxidation, emission and consumption of methane by
870 soils: A review, *Eur. J. Soil Biol.*, 37, 25-50.
- 871 Mayer, B., Humez, P., Becker, V., Nightingale, M., Ing, J., Kingston, A., Clarkson, C., Cahill, A.,
872 Parker, E., Cherry, J., Millot, R., Kloppmann, W., Osadetz, K., Lawton, D., 2015. Prospects and
873 Limitations of Chemical and Isotopic Groundwater Monitoring to Assess the Potential
874 Environmental Impacts of Unconventional Oil and Gas Development. *Procedia Earth and*
875 *Planetary Science* 13, 320-323.
- 876 Mayer, B., Humez, P., Nightingale, M., Clarkson, C., Cahill, A., Parker, B., Cherry, J., Millot, R.,
877 Kloppmann, W., Osadetz, K., Lawton, D., 2016. Tracing Fugitive Gas in Shallow Groundwater
878 in Areas of Unconventional Energy Resource Development, *Goldschmidt Conference*,
879 Yokohama.

- 880 Mercier M., Seguin A., 1939, L'épigraphie et les fontaines ardentes du Dauphiné, Bulletin de
881 l'Association Française des Techniciens du Pétrole, N°48-49.
- 882 Mörner N.-A., Etiope G., 2002, Carbon degassing from the lithosphere, *Global and Planetary*
883 *Change* 33, 185-203.
- 884 Parkin T.B., Venterea R.T., 2010, Sampling Protocols – Chapter 3 – Chamber-Based Trace Gas
885 Flux Measurements, In Sampling Protocols. R.F. Follett editor, 3-1 to 3-39.
- 886 Piret F.M., 1881, La Fontaine Ardente de Saint-Barthélémy (Isère) – Gaz naturel, charbon,
887 pétrole, Vincent and Perroux Eds, 76 p.
- 888 Roberts J.J., Wood R.A., Wilkinson M., Haszeldine S., 2015, Surface controls on the
889 characteristics of natural CO₂ seeps: implications for engineered CO₂ stores, *Geofluids* 15,
890 453-463.
- 891 Rogie J.D., Kerrick D.M., Chiodini G., Frondini F., 2000, Flux measurements of non-volcanic
892 emission from some vents in central Italy, *Journal of Geophysical Research*, vol. 105, No B4,
893 8435-8445.
- 894 Romanak K. D., Bennett P. C., Yang C., Hovorka S.D., 2012, Process-based approach to CO₂
895 leakage detection by vadose zone gas monitoring at geologic CO₂ storage sites, *Geophysical*
896 *Research Letters*, 39, L15405.
- 897 Romanak K., Yang C., Darvari R., 2017, Towards a method for leakage quantification and
898 remediation monitoring in the near-surface at terrestrial CO₂ geologic storage sites, *Energy*
899 *Procedia*, 114, 3855-3862.

- 900 Schroder I.F., Zhang H., Zhang C., Feitz A.J., 2016, The role of soil flux and soil gas monitoring
901 in the characterisation of a CO₂ surface leak: A case study in Qinghai, China, *International*
902 *Journal of Greenhouse Gas Control*, 54, 84-95.
- 903 Schroder I.F., Wilson P., Feitz A.F., Ennis-King J., 2017, Evaluating the performance of soil flux
904 surveys and inversion methods for quantification of CO₂ leakage, *Energy Procedia*, 114,
905 3679-3694.
- 906 Sigurdsson H., Devine J.D., Tchoua F.M., Presser T.S., Pringle M.K.W., Evans W.C., 1987,
907 Origin of the lethal gas burst from Lake Monoun, Cameroun, *Journal of Volcanology and*
908 *Geothermal Research* 31, 1-16.
- 909 Toutain J.P., Baubron J.C., 1999, Gas geochemistry and seismotectonics: a review,
910 *Tectonophysics*, 304, 1-27.
- 911 Voltattorni N., Lombardi S., 2010, Soil gas geochemistry: significance and application in
912 geological prospectings. In: Potocnik, Primoz (Ed.), *Natural Gas*. IX, pp. 183–204.
- 913 Von Arnold K., Weslien P., Nilsson M., Svensson B.H., Klemedtsson L., 2005, Fluxes of CO₂,
914 CH₄ and N₂O from drained coniferous forests on organic soils, *Forest Ecol. Manag.*, 210, 239-
915 254.
- 916 Weiss R.F., 1974, Carbon dioxide in water and seawater: the solubility of a non-ideal gas,
917 *Mar. Chem.*, 2, 203-215.
- 918 Werner C., Brantley S., 2003, CO₂ emissions from the Yellowstone volcanic system,
919 *Geochemistry Geophysics Geosystems*, 4(7), 1061, doi:10.1029/2002GC000473.

- 920 Wiesenburg D.A., Guinasso N.L., 1979, Equilibrium Solubilities of Methane, Carbon
921 Monoxide, and Hydrogen in Water and Sea Water, *Journal of Chemical and Engineering*
922 *Data*, 24(4), 356-360.
- 923 Zazzeri G., Lowry D., Fisher R.E., France J.L., Lanoisellé M., Nisbet E.G., 2015, Plume mapping
924 and isotopic characterisation of anthropogenic methane sources, *Atmospheric Environment*
925 *110*, 151-162.

926 **Figure captions.**

927 Figure 1 A: Location of methane-rich gas seeps in the W-subalpine chains (Blavoux *et al.*,
928 1990, Etiope *et al.*, 2010, Gal *et al.*, 2017a) plotted on the geological map of France (1:1
929 000 000, BRGM). Geological formations in blue range from Lower Jurassic to Upper
930 Cretaceous; B: close-up view of the Fontaine Ardente du Gua gas seep: different views in
931 2015 and 2016 showing the bare soil zone where CH₄ emissions occur and the pebbly area
932 where the Vernant creek usually flows (arrow indicates the location of the Fontaine Ardente
933 corresponding to the location of former wellhead of FA2 borehole); C: location of the
934 sampling points in 2015 and in 2016 (satellite photograph from Google Earth).

935 Figure 2 : whisker plots for the 2015 and the 2016 surveys. CO₂, O₂ and CH₄ soil gas
936 concentrations data: GC measurements (2015) and corrected IRGA measurements (2016).
937 Other soil gas concentrations data: GC measurements only. Flux data are only available for
938 2016 (see supplementary information for details about flux calculation).

939 Figure 3: A: O₂ vs CO₂ binary plot; B: location of points as a function of the slope of the O₂ vs
940 CO₂ relationship (inset: detailed location around the main vent). Blue circled points
941 correspond to points labeled in **Error! Reference source not found.** C: left: O₂ vs N₂ binary
942 plot showing two data distributions; equations of each linear fit are indicated; yellow points
943 correspond to 2015 data plotting between the two distributions; right: location of points as a
944 function of the slope of the O₂ vs N₂ relationship: grey dots for the orange linear fit (N₂+O₂
945 depletion line = dilution line); white dots for green linear fit (O₂ depletion line = respiration
946 line).

947 Figure 4: A: CH₄ vs. O₂ binary plot; B: CH₄ vs. CO₂ binary plot. Plots are drawn using filtered
948 data by reference to the N₂+O₂ depletion line and the O₂ depletion line defined in Figure 3.

949 The map (C) locates the points as defined by the linear fits in black and blue lines in the
950 binary plots (points in black and blue respectively).

951 Figure 5: A: left: relation between CO₂ and CH₄ fluxes for all measurements; right: location of
952 the measurements; B: left: relation between CO₂ and CH₄ fluxes for low CH₄ fluxes (lesser
953 than 1 g/m²/h); the linear fit corresponds to the data plotted in grey circles; right: map
954 showing the geographical distribution of high and low CO₂ fluxes (high fluxes are divided into
955 3 subgroups).

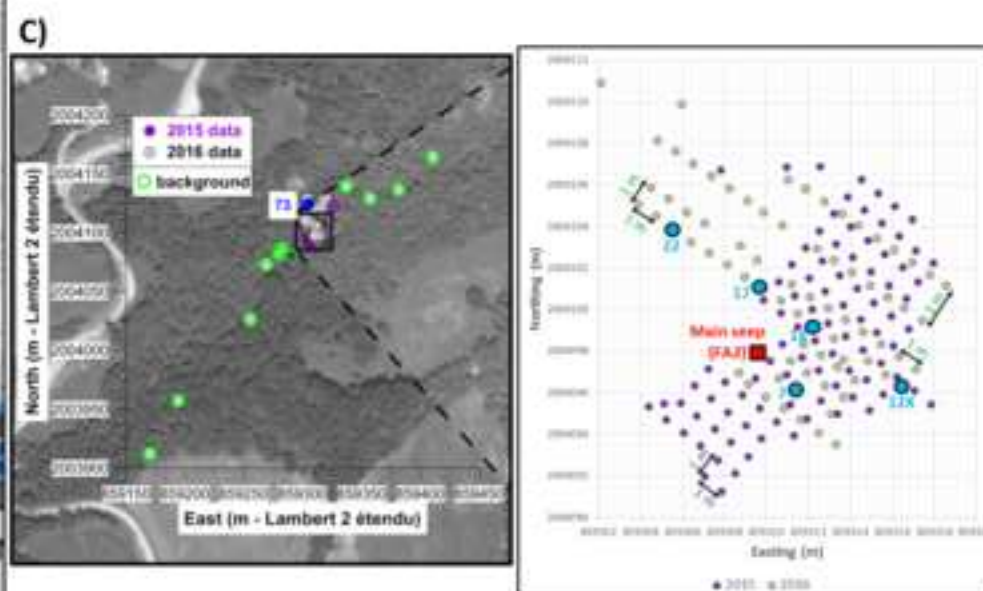
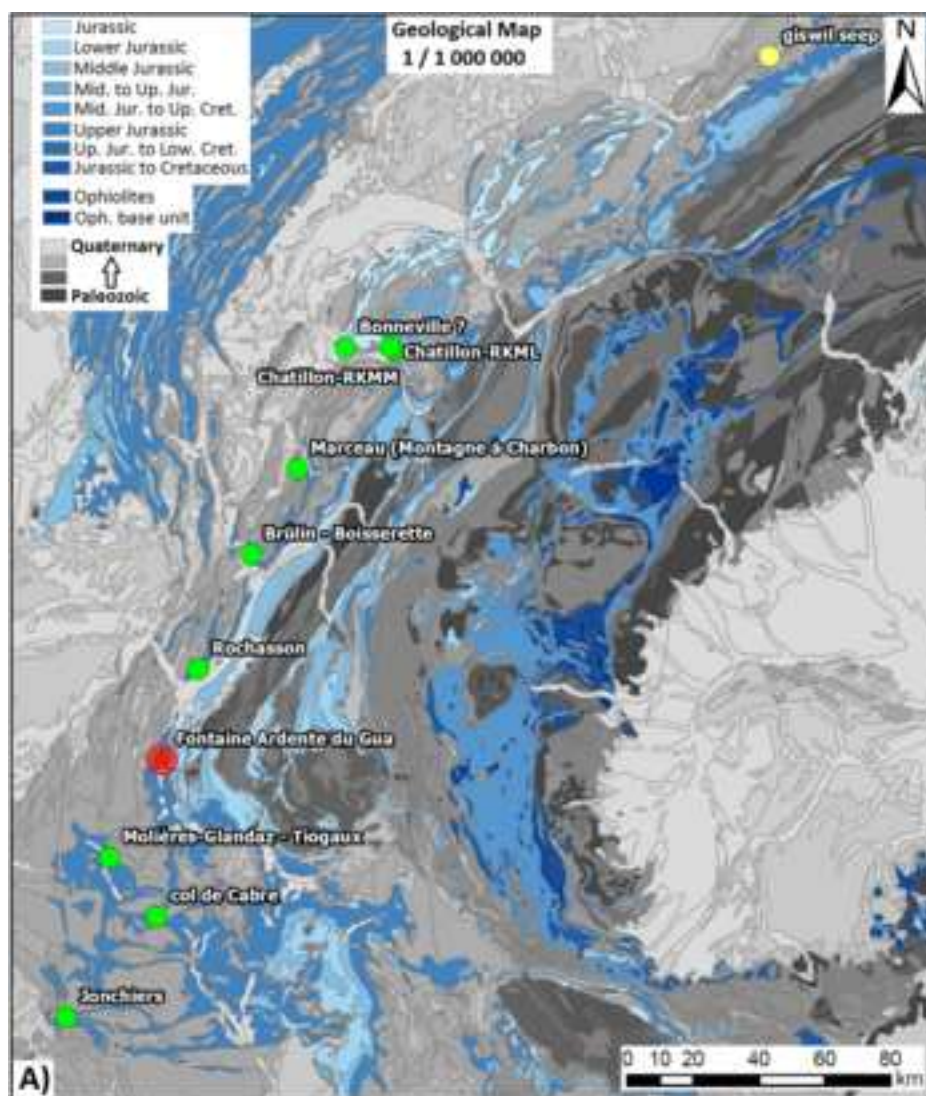
956 Figure 6: A: O₂ depletion as a function of CO₂ flux or CH₄ flux; B: geographical location of
957 points showing O₂ depletion.

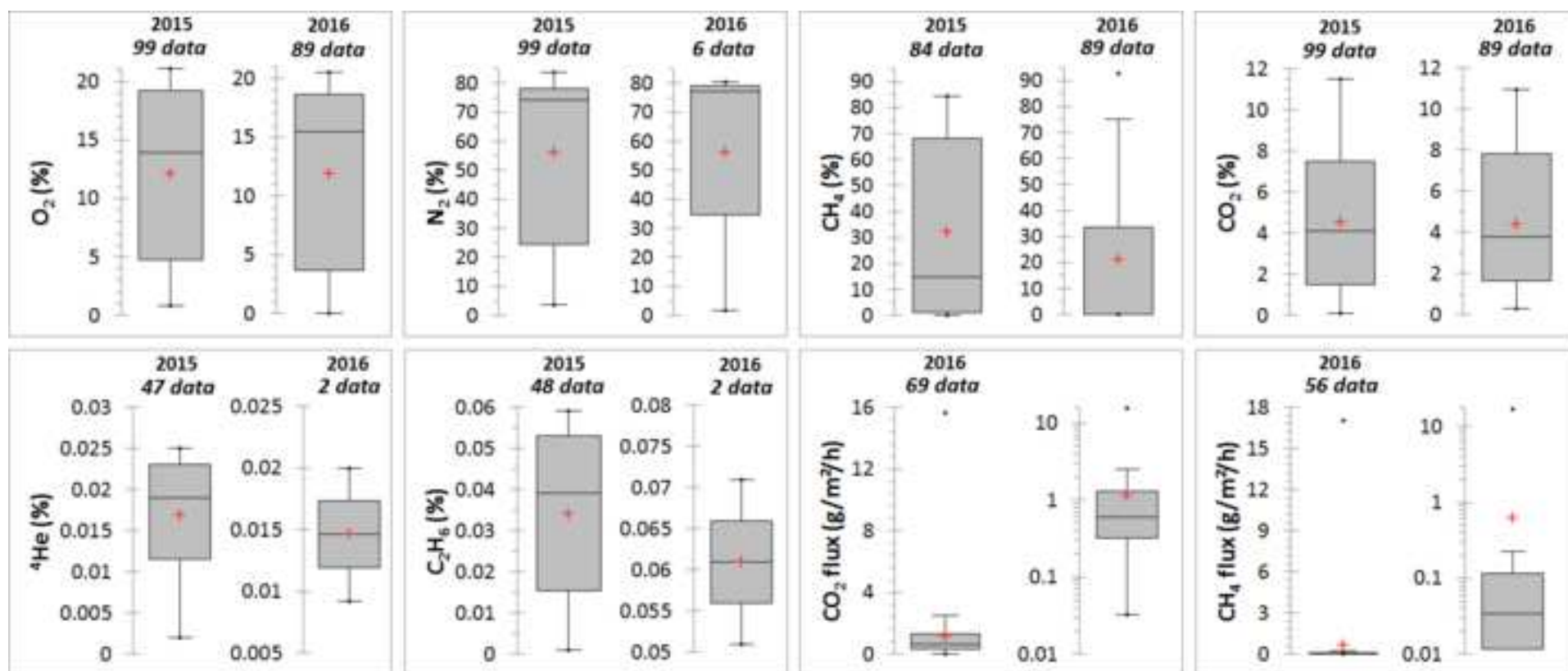
958 Figure 7: typology of CO₂ concentration increase and CH₄ concentration increase (shaded
959 area) in the chamber during flux measurement. Blue lines represent the fits used for flux
960 calculations; red lines represent the fits that are not used for flux calculations.

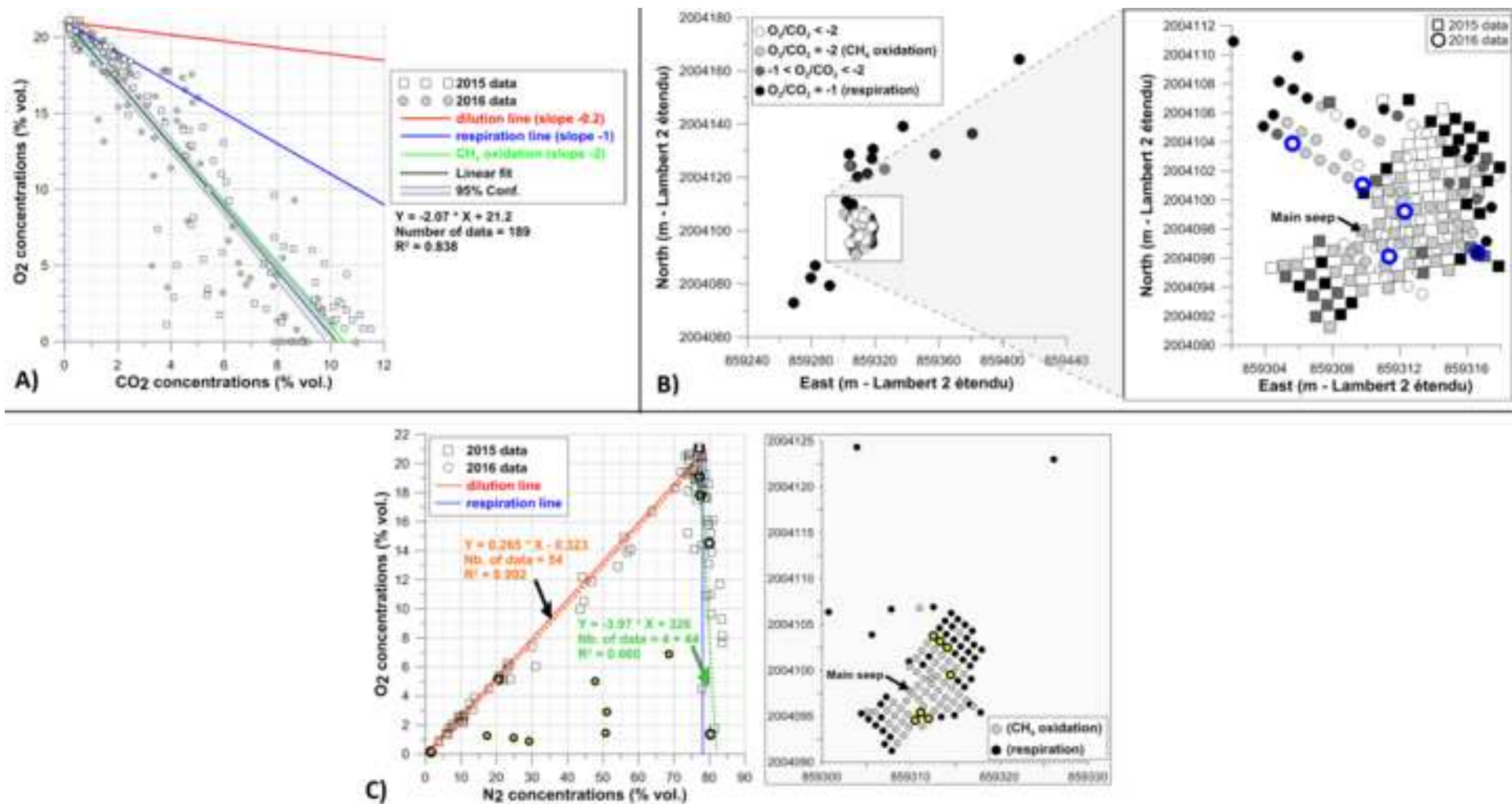
961 Figure 8: chrono-photography of the “Fontaine Ardente” gas seep in the manner of Étienne
962 Jules Marey, French physiologist (end of XIXth) – 06 October 2016.

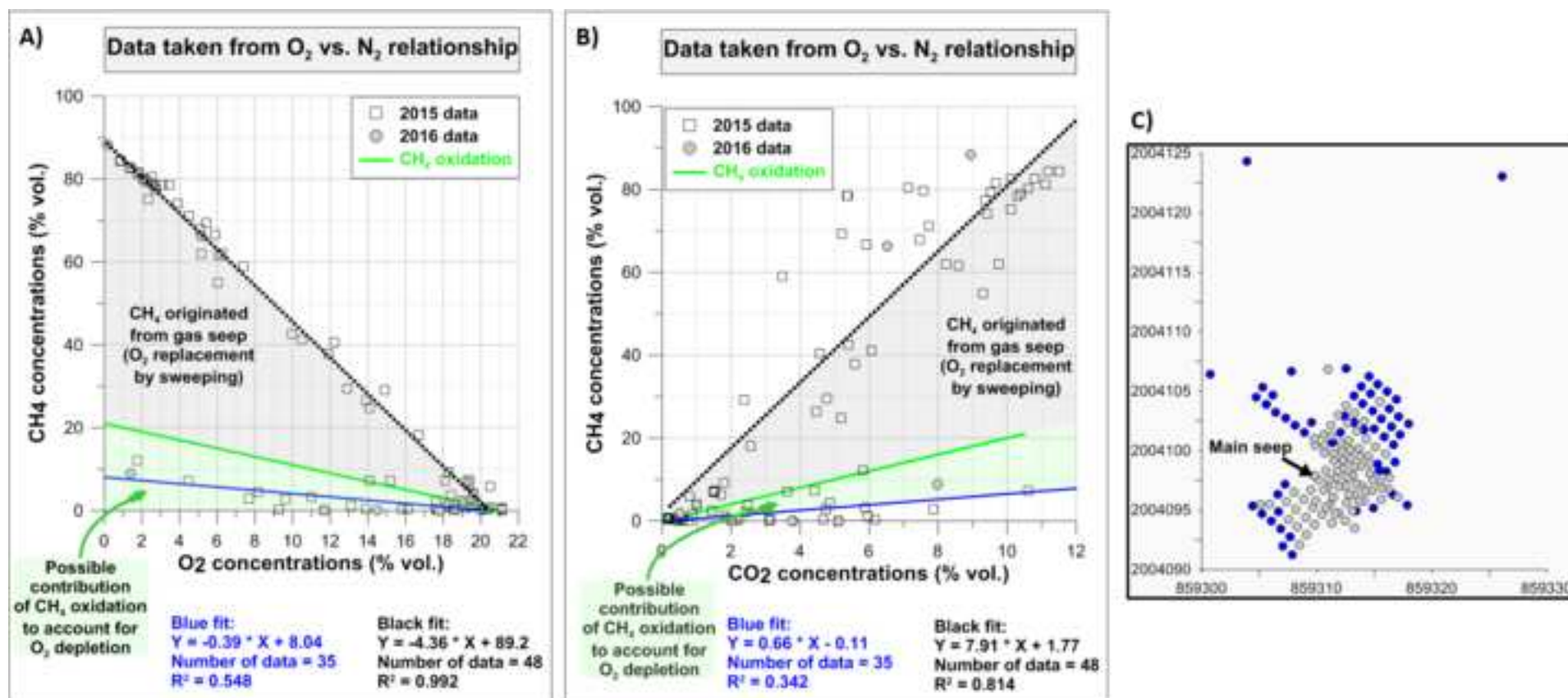
963 Figure 9: contour maps of soil gas species (concentrations in % vol.) and soil gas flux (in
964 g/m²/h); kriging is done using data reported in supplementary information. Locations of
965 measurements are reported on each map: area investigated during soil gas measurements:
966 400 m² (20x20 m); area investigated during soil flux measurements: 240 m² (dashed polygon
967 in bottom maps). The red dot indicates the location of the “Fontaine Ardente”. The striped
968 area in bottom right map shows the emplacement of the Vernant creek bed; the dark grey
969 area shows the area (84 m²) used for quantification of the gas emissions (no flux
970 measurement possible in the light grey area: old concrete plugs from former FA2 borehole).

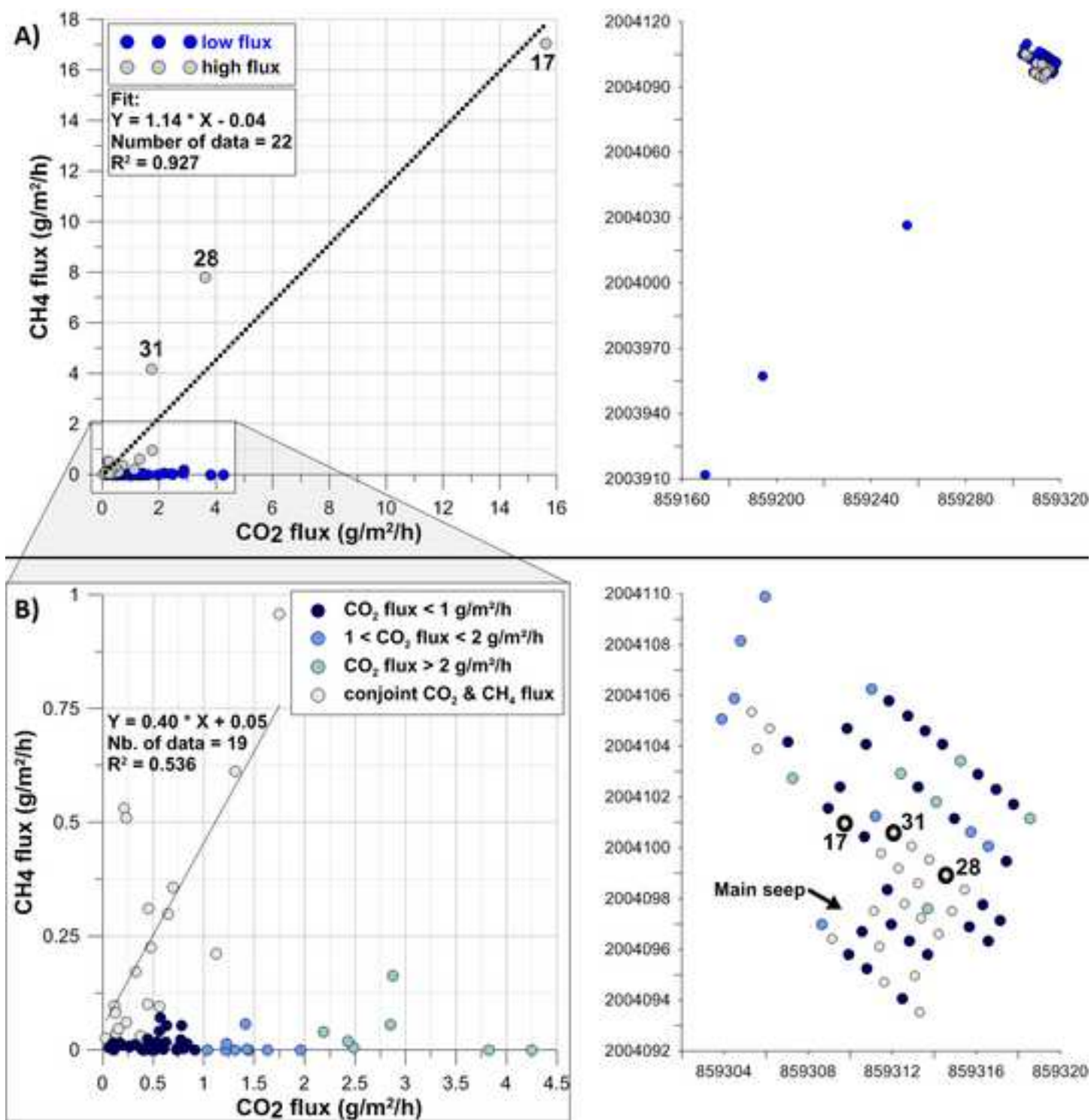
971 Figure 10: infrared camera monitoring using specific lens sensitive to CO₂ (FLIR); the picture
972 in the right shows the conditions of monitoring, with shooting of the CO₂ plume just above
973 the flame (as can be seen in the background). The insets in the left show, from bottom to
974 top: the CO₂ plume directly issued from the burning seep; the CO₂ plume reaching the first
975 branches in the trees (3 to 4 m above ground); the dilution of the CO₂ plume at around 5 m
976 height.











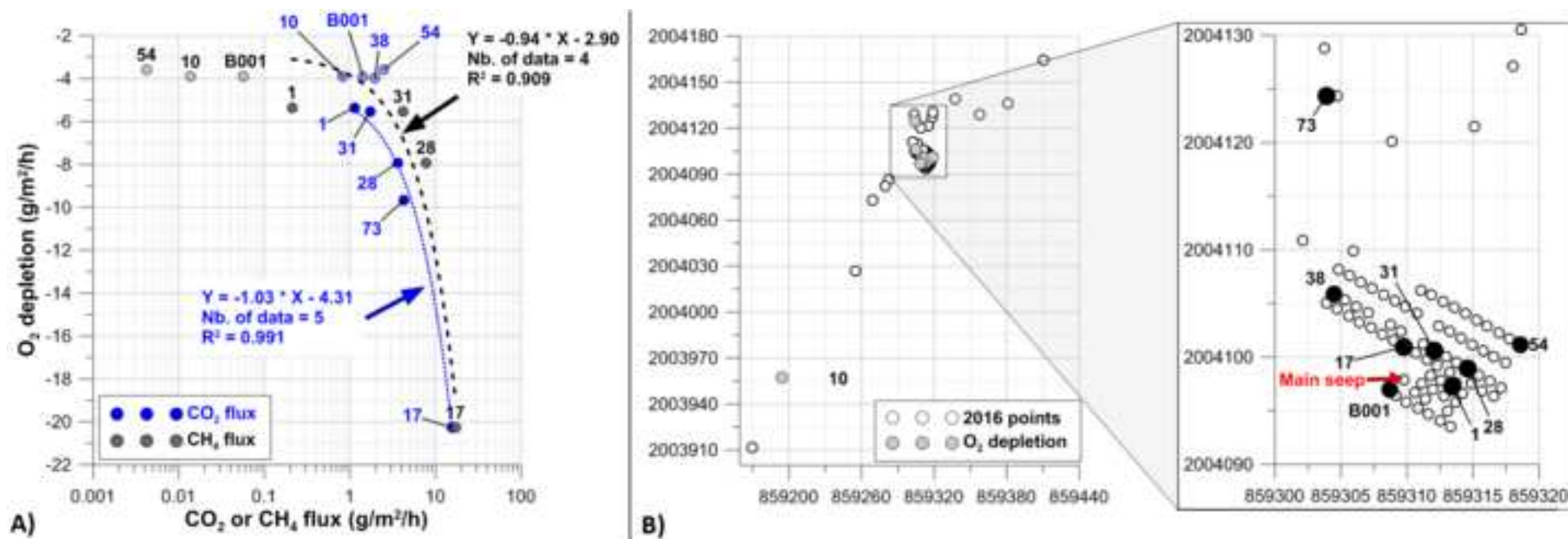


Figure 7

[Click here to download high resolution image](#)

Accepted Manuscript

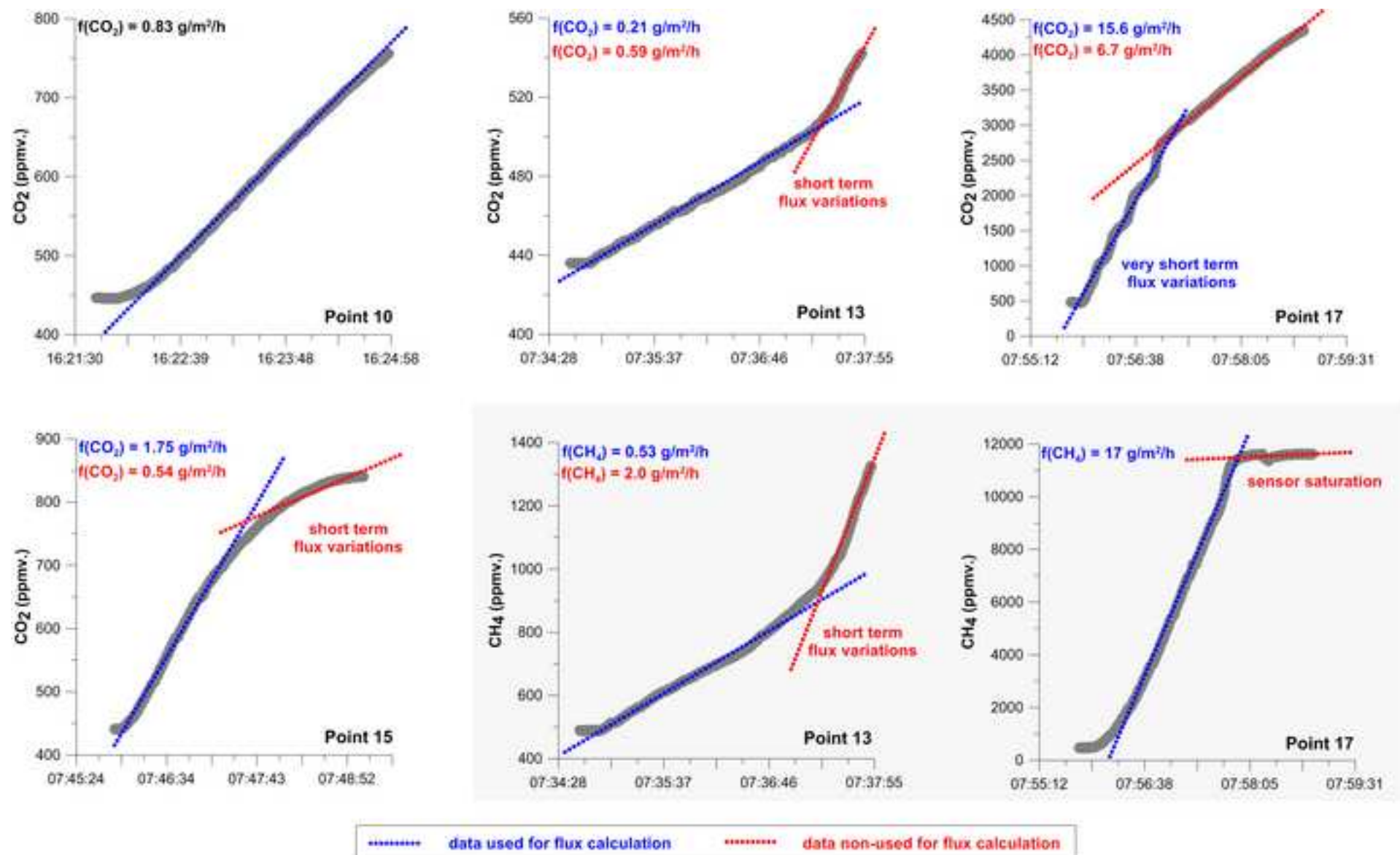




Figure 9
[Click here to download high resolution image](#)

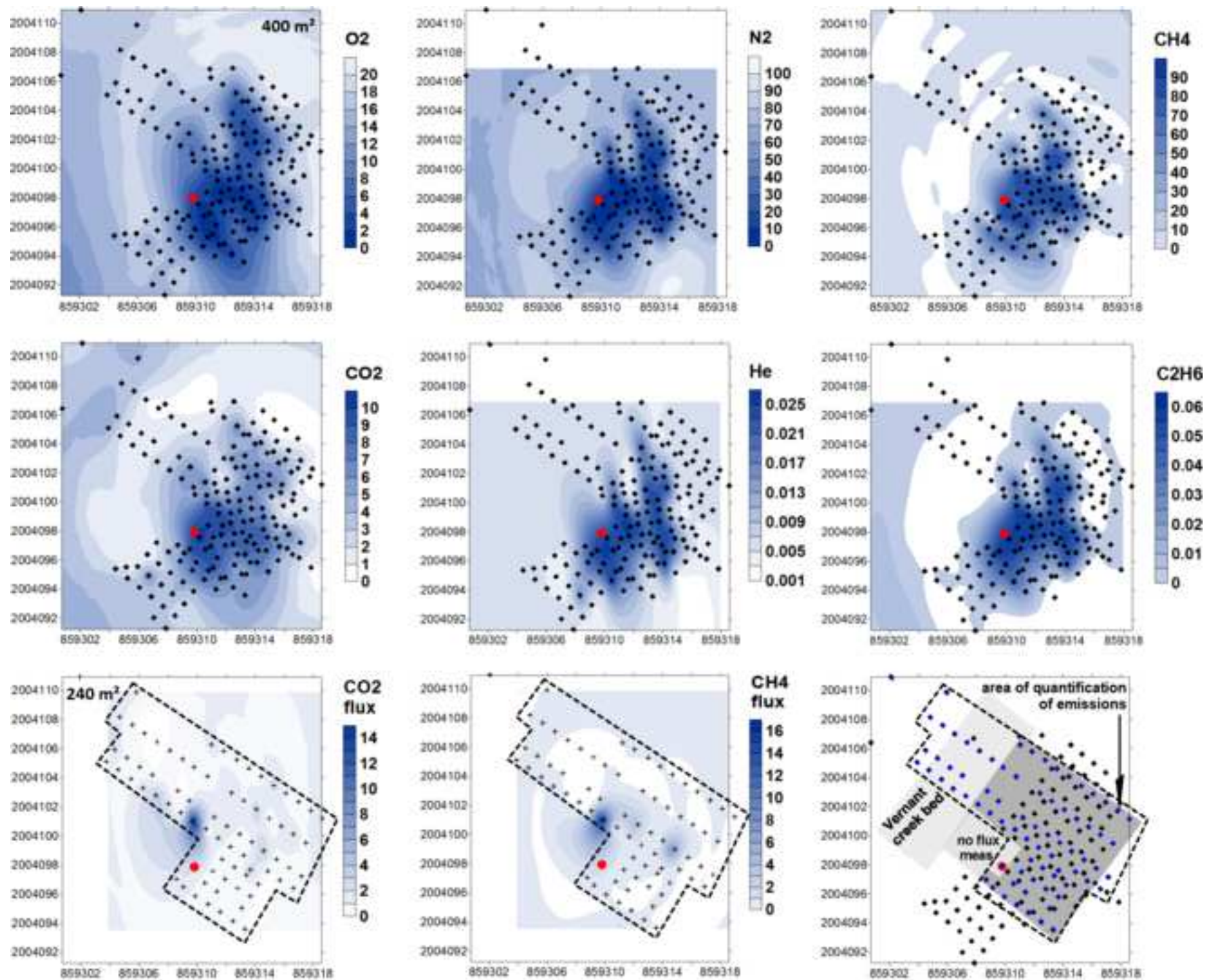
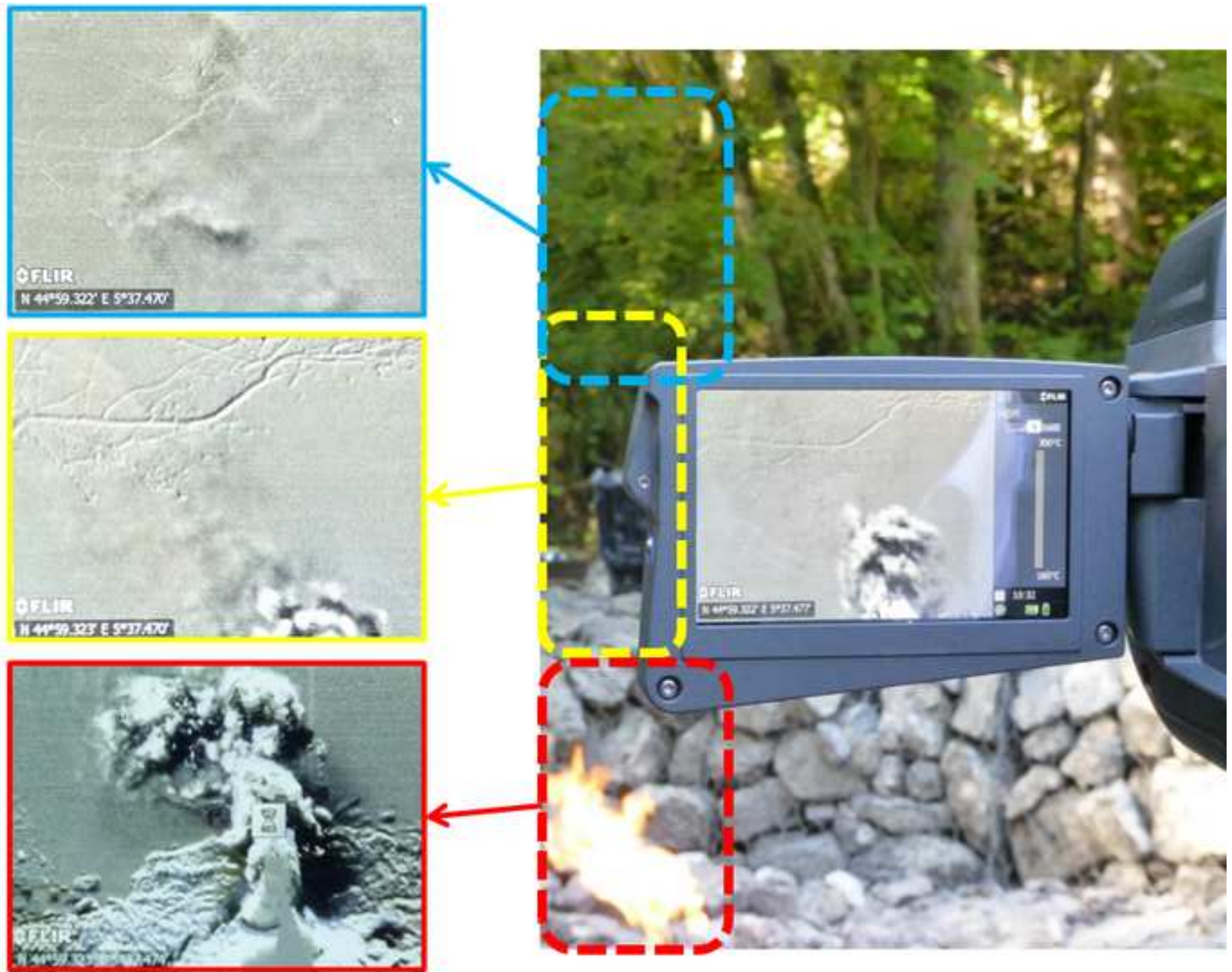


Figure 10
[Click here to download high resolution image](#)



Supplementary material

A.1 Methods

A.1.1 Soil gas measurements

In 2016, only IRGA device was used to monitor soil gas concentrations. In order to take into account of deviations from the gas concentrations resulting from these IRGA measurements, IRGA data were calibrated against gas chromatography data. Six samples, representative of the whole CH₄ concentration range as monitored in the field (from 0 to 77% vol.), were taken in appropriate containers (Isotubes®) and analyzed in the lab (Thermo Trace GC). This allowed correcting the bias inherent to IRGA analyses at high concentrations and to homogenize the 2016 dataset in view of comparing 2015 and 2016 campaigns. The same procedure was applied to CO₂ and O₂ gas concentrations. R² correlation coefficients between IRGA field measurements and laboratory analyses are 0.9952, 0.9941 and 0.9992 for CO₂, O₂ and CH₄ respectively (n=6). The mean error, evaluated using the slope of the linear fit between IRGA field measurements and lab measurements, is close to +4.8% for CO₂ (field data are slightly higher), -16.5% for CH₄ (field data are strongly underestimated) and +2.8% for O₂ (field data are slightly higher).

A.1.1 Soil gas flux measurements

The flux is calculated by considering the linear build-up of the gas concentration in the chamber during 3 minutes and by determining the initial slope of the gas concentration vs. time relationship, as described by many authors (*e.g.* Chiodini *et al.*, 1998; Etiope *et al.*, 2013a, and references therein). Fluxes were calculated according to the equation detailed by Lewicki *et al.* (2005) to correct the influence of pressure and temperature changes.

Uncorrected and P-T-normalized CO₂ fluxes only differ by 0.65% as a mean (uncorrected fluxes are slightly higher), the whole range being between -0.24% and +1.41% (69 CO₂ flux measurements). The influence of temperature and pressure changes is thus very low in the present case and the dataset can be considered as non- temperature or pressure dependent.

Not all the fluxes were calculated using the initial slope obtained from the 3 minutes duration of the build-up of gas concentrations inside the chamber. Contrarily to soil gas concentration measurements, some flux measurements were subject to short time scale variations of both the CO₂ and the CH₄ fluxes. In such cases, the fluxes have been calculated considering the linear fit that was prevailing during the major part of the acquisition. These short term variations concerned only a minor part of the data (respectively 17 of 69 CO₂ flux measurements and 12 of 56 CH₄ flux measurements).

Oxygen concentration decreases have been monitored at 10% of the monitoring points – this may be a consequence of a too short duration of the measurement sequence, typically set at 3 minutes in order to remain in the domain of linear increase (or decrease) of the gas concentrations. This may also be simply the consequence of low soil O₂ (progressive dilution by an oxygen-poor gas in the chamber). The point (label 17 in Figure 1) where O₂ concentration decrease was at maximum is also the unique point where the CH₄ sensor reached saturation within only 2 minutes thus the linear regression from which the flux is calculated was established only over this 2 minutes period.

As earlier reported (Chiodini *et al.*, 1998; Bloomberg *et al.*, 2012; Sanci *et al.*, 2009), soil moisture may also have a strong influence on the evaluation of gas emissions. The most obvious influence is via soil biological activity. In the present case – CH₄-rich seepage – this influence may eventually exist for the CO₂ gas phase but is less obvious for the CH₄ gas phase

as there are no potentially CH₄-emitting wetlands in the vicinity of the investigated sites. Field monitoring was performed during summertime thus the influence of humidity may be expected as reduced. Soil moisture directly influences soil gas concentrations through gas dilution by the water vapor content of the gas phase. Values of relative humidity of the air inside the chamber generally fall between 55% and 70% after the purge of the flux chamber depending on the hour of the day. Humidity variations measured during 3 minutes did not exceed +10% of the initial value and the observed maximum value was 75%. No apparent influence of moisture on CH₄, CO₂ or O₂ measurements has been stated during the graphical examination of raw data. This is consistent with the statement reported by Parkin and Venterea (2010). They found that an increase in relative humidity within a chamber from 0% to 100% will dilute the gas by only 3.05%. In the present case, it may be postulated that the influence of gas dilution will be considerably lower than 1% and can therefore be reasonably neglected.

Last, permanent visualization of the flow rate inside the system did not highlight any biases linked to the system itself during the measurement session. Nonetheless, such issues were sometimes encountered during CH₄ and H₂ measurements. A purge time is allocated between two measurements in order to refresh the air inside the system. The recovery of near atmospheric values is established in between 1 and 3 minutes for CO₂ and O₂. This may be somewhat longer for CH₄ as some memory effect on the sensor may delay the return to near zero values in case the atmospheric CH₄ background is elevated. This residual effect, sometimes reaching 200 to 300 ppm, may have induced some underestimates of CH₄ fluxes (no flux was measured instead of measuring a small flux).

A.2 Statistics

As shown by Figure A.2.a, the whole dataset is skewed for all gases. Consequently, the data are not distributed under normal law (Gaussian distribution) nor lognormal law (log-transformed data show Gaussian distribution). The situation is better when the dataset is reduced; He and C₂H₆ concentration distributions are then normal (p-values of 0.100 and 0.188 resp. using Kolmogorov-Smirnov test) and CO₂ and CH₄ fluxes distributions rather log-normal (p-values of 0.929 and 0.729 resp.). As the data measured hundreds of meters from the Fontaine Ardente main seep are likely not influenced by the gas seep (background data), the use of a dataset restricted to the vicinity of the seep (square of 20 m of side) is a way to better define data distribution. The only change by using sub-sampled dataset is the appearance of a slight tendency for CO₂ concentration to follow a normal distribution (p-value of 0.05). Another change is a higher p-value for CO₂ fluxes (0.965).

From Figure A.2.a it can be seen that data distribution is frequently bimodal. These poly-modal data distributions may exist *e.g.* for O₂ concentrations with a cut-off at 6.8% vol. or for CH₄ concentrations with a cut-off at 4.36%. One distribution is linked to the existence of the gas seep and the second is linked to common biological processes in soils. Consequently, the use of arithmetic parameters (mean and standard deviation), defined for a normal distribution, for the calculation of threshold levels cannot be used.

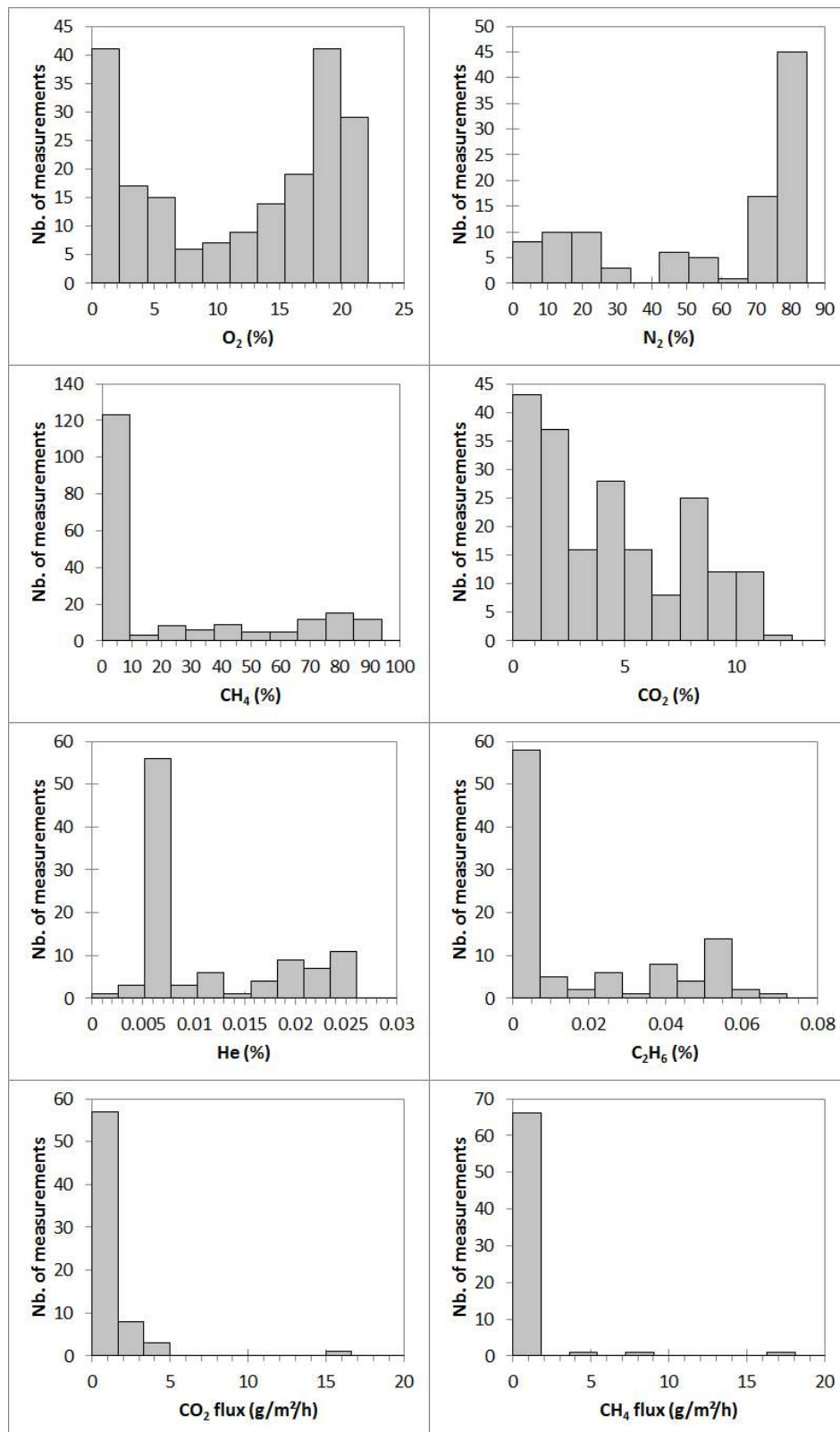


Figure A.2.a: histograms of soil gas data (2015 and 2016 data) and soil flux data (2016)

showing heterogeneous data distribution.

Here we refer to the quantile-quantile (Q-Q) plots to define threshold values (Figure A.2.b). The log-transformed data help to highlight changes in data distribution associated with strong deviations in the slope of the Q-Q plots. Anomaly thresholds are defined as follows: 17.5% vol. (O_2), 3.8 and 7.5% vol. (CO_2), 65% vol. (CH_4), 190 ppm (He) and 360 ppm (C_2H_6). As CO_2 and CH_4 flux data are linearly distributed, a clear definition of a threshold is not possible albeit deviations around the 0.25 quantile may have some significance (1.23 and 0.21 $g/m^2/h$ resp.). A reference to the thresholds obtained using the basic approach (mean + 2SD) gives levels of 5.14 and 5.66 $g/m^2/h$ respectively and such levels are not meaningful (only 1 point is above the CO_2 threshold and 2 points above the CH_4 flux threshold). Interestingly, the CO_2 and O_2 soil gas threshold levels (3.8% and 17.5%) are in good agreement with the pivot values defined in Figure 3 thus giving more confidence on the concentrations from which influence of the gas seep can be noticed.

Prior to establishing contour maps, variograms were calculated for each parameter on a restricted dataset (data falling in the 20x20 m side square around the seep). Results are given in Figure A.2.c and show the parameters of variogram calculation used for krigged maps.

Figure A.2.d presents classed post maps built using threshold levels given in Figure A.2.b.

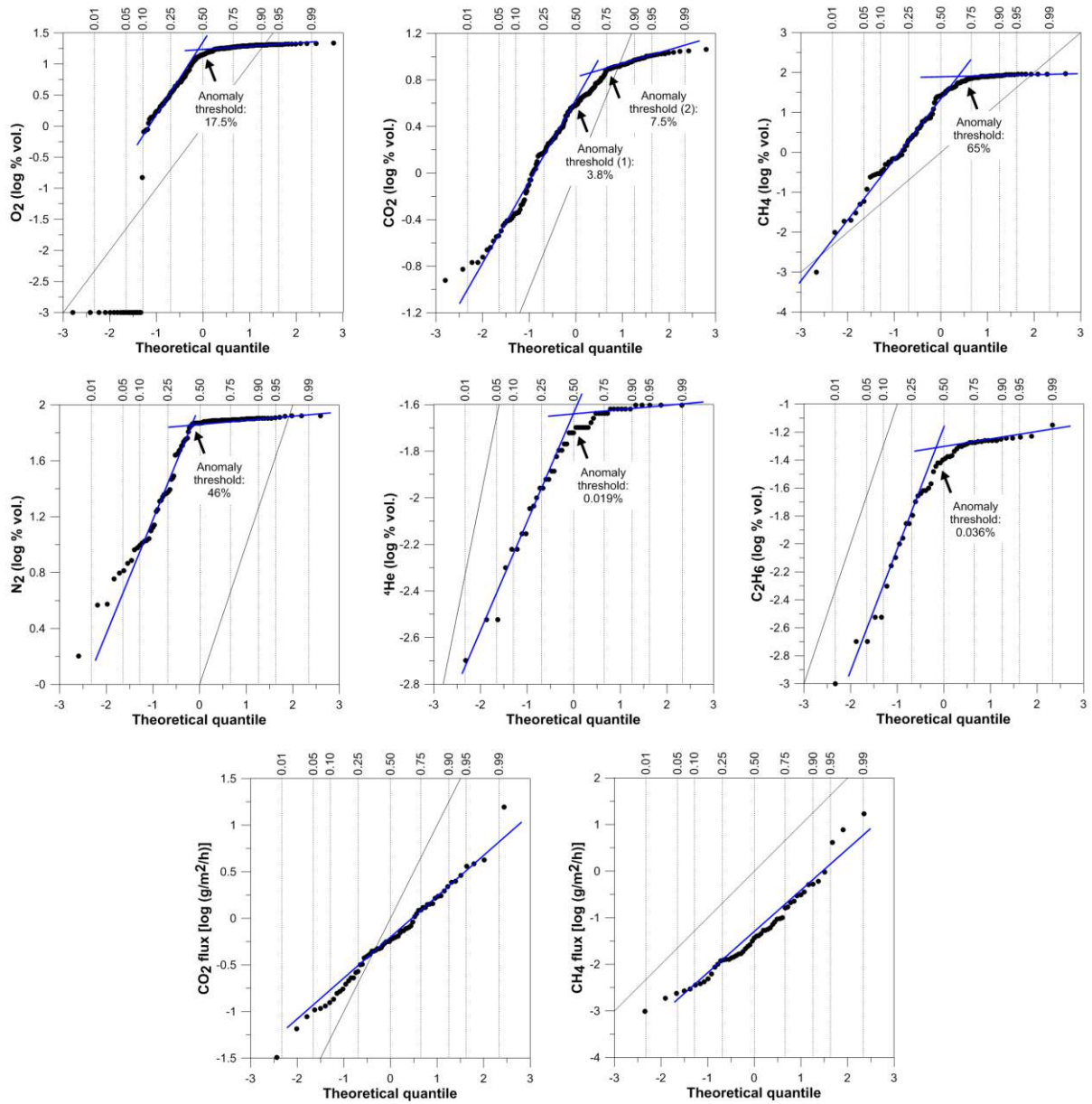


Figure A.2.b: quantile-quantile plots calculated for all the soil gas species and the CO₂ and CH₄ soil gas fluxes.

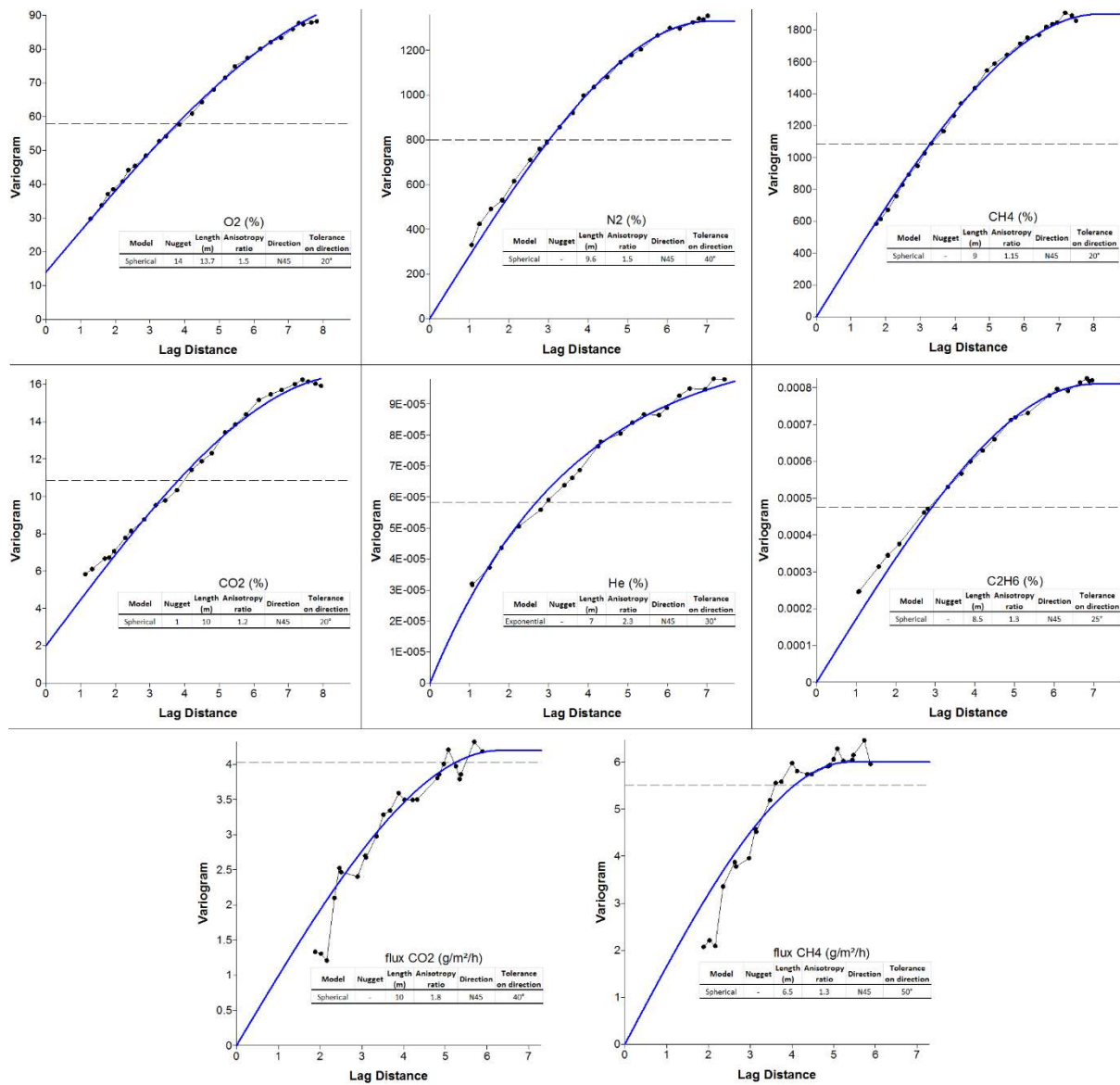


Figure A.2.c: variograms calculated for all the soil gas species and the CO₂ and CH₄ soil gas fluxes. Lag distance in meters.

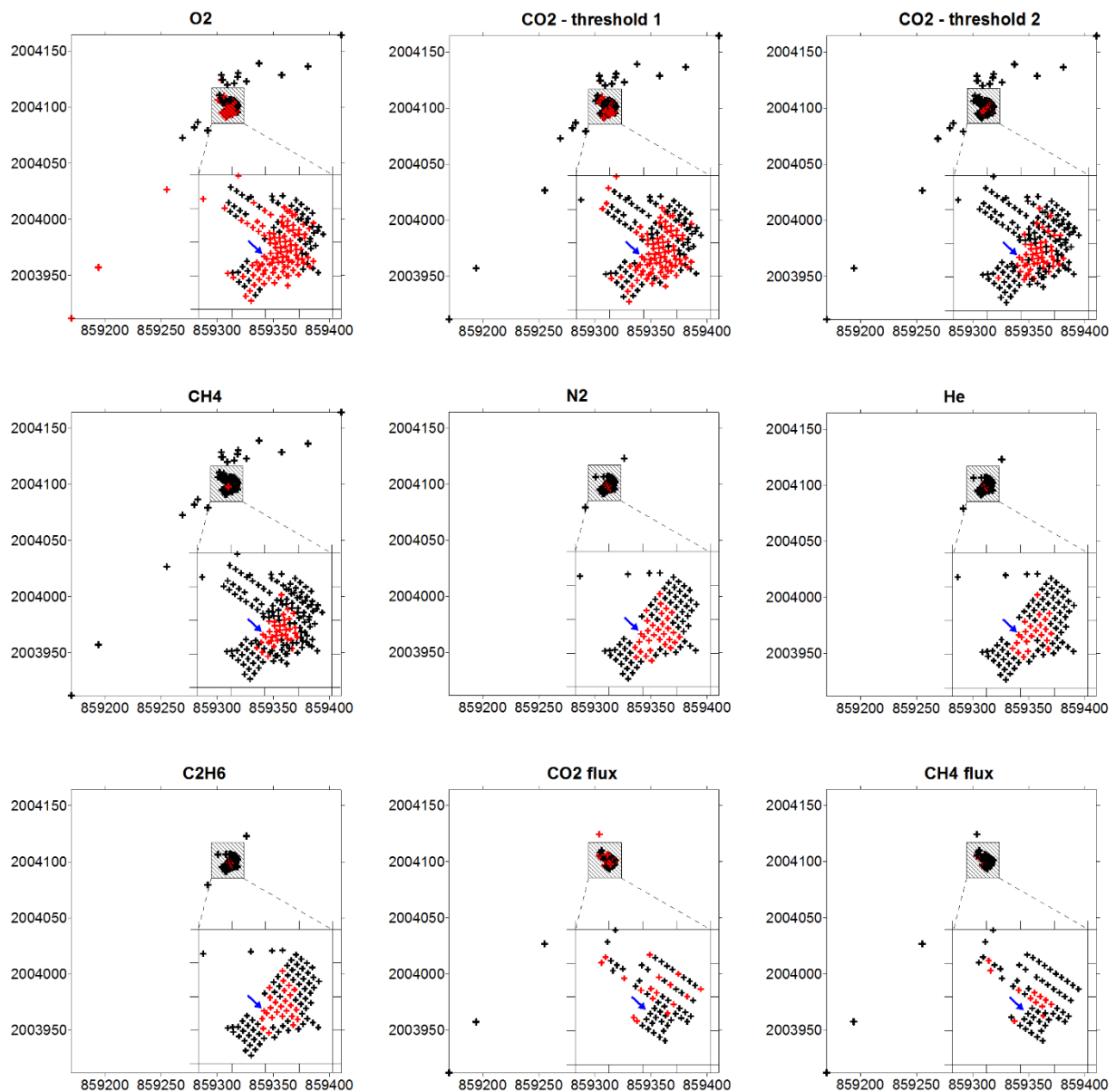


Figure A.2.d: classed post maps for the monitored parameters; insets in each map shows a detailed view of the 20x20 m side square near the gas seep. The blue arrow indicates the location of the Fontaine Ardente main seep. Red dots correspond to points that are above the threshold values defined in the text and in Figure A.2.b.

Supplementary material – References (if not cited in main text)

Lewicki J.L., Bergfeld D., Cardellini C., Chiodini G., Granieri D., Varley N., Werner C., 2005, Comparative soil CO₂ flux measurements and geostatistical estimation methods on Masaya volcano, Nicaragua, *Bull. Volcanol.*, 68, 76-90.

Sanci R., Panarello H.O., Osters H.A., 2009, Assessment of soil moisture influence on CO₂ flux: a laboratory experiment, *Environ Geol*, 58, 491-497.